Adaptive Friction Compensation for Servo Mechanisms

J. Wang, S. S. Ge, and T. H. Lee

Department of Electrical and Computer Engineering,
National University of Singapore,
Singapore 117576
Email: elegesz@nus.edu.sg

Abstract

Friction exists in all machines having relative motion, and plays an important role in many servo mechanisms and simple pneumatic or hydraulic systems. In order to achieve high precision motion control, accurate friction modeling and effective compensation techniques have to be investigated. In this chapter, we shall present a systematic treatment of adaptive friction compensation techniques from both engineering and theoretical aspects. Firstly, a comprehensive list of the commonly used classical friction models and dynamic friction models is presented for comparison and controller design. Then, by considering the position and velocity tracking control of a servo mechanism with friction, adaptive friction compensation schemes are given based on the LIP static friction model and dynamic LuGre model respectively. Finally, extensive simulation comparison studies are presented to verify the effectiveness of the proposed methods.

1 Introduction

Friction exists in all machines having relative motion, and plays an important role in many servo mechanisms and simple pneumatic or hydraulic systems. It is a natural phenomenon that is hard to model, if not impossible. As friction does not readily yield to rigorous mathematical treatment, it is often simply ignored for the lack of control tools available or regarded as a phenomenon unworthy of discussion. In reality, friction can lead to tracking errors, limit cycles, and undesired stick-slip motion. Engineers have to deal with the undesirable effects of friction though lack of effective tools to make it easier to handle.

All surfaces are irregular at the microscopic level, and in contact at a few asperity junctions. These asperities behave like springs, and can deform either elastically or plastically when subjected to a shear force. Thus, friction will act in the direction opposite to motion and will prevent true sliding from taking place as long as the tangential force is below a certain stiction limit at which

the springs become deformed plastically. At the macro level, many factors affect friction such as lubrication, velocity, temperature, force orthogonal to the relative motion and even the history of motion. In an effort to deal with the undesired effects of friction effectively, many friction models have been presented in the literature relevant to friction modeling and control.

Friction can be classified into two categories: static and dynamic. Conventionally, friction is modeled as a static function of velocity and the externally applied force. The notorious components in friction are stiction and Coulomb friction forces, which are highly nonlinear functions of velocity although bounded, and cannot be handled by linear control theory. Traditionally, friction is treated as a bounded disturbance, and the standard PID (Proportional-Integral-Derivative) algorithm is used in motion control. However, the integral control action may cause limit cycles around a target position and result in large tracking errors. If only PD control is employed, then friction will cause a finite steady-state error. Though high gain PID can reduce the steady–state position error due to friction, it often causes system instability when the drive train is compliant [18]. Thus, in order to achieve high precision motion control, friction must be appropriately compensated for. Friction compensation can be achieved based on a reasonable accurate model for friction. However, it is difficult to model friction because it depends on many factors such as velocity, position, temperature, lubrication and even the history of motion. Direct compensation of friction is desirable and effective in motion control. However, it is difficult to realize in practice because of the difficulty in obtaining a true representative parametric model. For controller design, the parametric model should be simple enough for analysis, and complex enough to capture the dominant dynamics of the system. If the model used is too simple, such as the simple Coulomb friction and viscous friction model, then there is the possibility of overcompensation resulting from estimation inaccuracies [12]. Adaptive friction compensation schemes have been proposed to compensate for nonlinear friction in a variety of mechanisms [1, 12], but these are usually based on the linearized model or a model which is linear-in-the-parameters for the problems under study. Each model captures only the dominate friction phenomena of the system and may exhibit discrepancies when used for other systems where other friction phenomena appear.

Although static-model-based adaptive friction compensation techniques have been proposed in the literature [4, 13, 15, 19], the results are not always satisfactory in applications with high precision positioning and low velocity tracking. Several interesting properties observed in systems with friction cannot be explained by static models because the internal dynamics of friction are not considered. Examples of the dynamic properties include: stick-slip motion, presliding displacement, Dahl effect and friction lag. Accordingly, dynamic friction models are preferred for the development of advanced friction compensation schemes. A notable dynamic friction model which captures

all the static and dynamic characteristics of friction is the dynamic LuGre model proposed in [13]. The necessary and sufficient conditions for passivity of the LuGre model was recently given in [6].

When using the dynamic LuGre friction model, controller design becomes difficult because (i) the friction parameters appear in a nonlinear fashion, and (ii) the system's internal state z, which depends on unknown parameters, is not measurable. Based on the LuGre model [13], several nice model-based controllers have been developed. Under the assumption of known system parameters and functions, a model-based controller was presented in [13] with the unmeasurable friction state being estimated by an observer which is driven by the tracking error. Two globally stable model-based adaptive friction compensation schemes were presented in [15] for structured variations by assuming that changes in friction are mainly due to either changes in the normal force that only affects proportionally the static friction characteristics, or temperature variations affecting uniformly both static and dynamic parameters. Accordingly, the resulting schemes adapt only one single parameter. In [32], using a dual-observer structure for the internal friction state estimation, two elegant controllers were presented for the following two cases: (i) unknown friction coefficients with known inertia parameter and known friction characteristic function, and (ii) known friction characteristic function with unknown multiplying coefficient for handling nonuniform variation in the friction force and normal force variations. Case (ii) is an alternative to the solution given in [15].

Due to its uniform approximation ability to any continuous nonlinear functions, there has been considerable research interest in neural network (NN) control of nonlinear systems, and some have been applied to systems with friction, which are usually difficult to model. In [14], an adaptive NN controller was proposed, where the NN was used to parameterize the nonlinear characteristic function of the dynamic friction model which may be a function of both position and velocity with known system parameters. In [25], a reinforcement learning based NN adaptive control scheme was applied to compensate for stick-slip friction for tracking control of a 1-DOF mechanical system with guaranteed high precision and smoothness of motion. In [21], both model-based and NN-based adaptive controllers were investigated for dynamic friction, where the friction model for controller design is given in an easy-to-use linear-in-the-parameters (LIP) form. By considering the dynamic LuGre model, two NN-based adaptive friction compensation schemes have recently been proposed in [22]. One is for the unknown nonlinear friction characteristic function in the LuGre model, and the other is for completely unknown parameters in the LuGre model.

Though adaptive control of systems with smooth nonlinearities has made remarkable progress in recent decades, they are not directly applicable to systems with frictions, which is a nonsmooth nonlinearity. Control of such nonlinearities has been a tough challenge academically and practically. In

this chapter, we shall present a systematic treatment of adaptive friction compensation techniques from both engineering and theoretical aspects.

Firstly, we will give a detailed account of the commonly used friction models including their history and properties. Several classical static friction models and dynamic friction models are described. As a result, we shall present a simple linear-in-the-parameters (LIP) friction model that captures most of the observed static friction phenomena of velocity, and is easy to use for controller design. As the space of primitive functions increases, the model becomes more complete and representative, and thus reduces the possibility of friction overcompensation resulting from estimation inaccuracies caused by simplified friction model structures, such as simple Coulomb friction and viscous friction models. The properties of the dynamic LuGre model are also discussed in detail for controller design. The LuGre model used in our design accounts for both the position and velocity dependence of the friction force.

Secondly, by considering the position and velocity tracking control of a servo mechanism with friction, adaptive friction compensation schemes are presented based on the static friction model and dynamic LuGre model. For static friction model based compensation, the emphasis is on a unified adaptive controller based on our proposed LIP friction model and the study of effects in augmenting the space of basis/primitive functions. For the dynamic LuGre model, in order to provide good control performance, new adaptive controllers are presented, combining NN parameterization, dual-observer for state estimation/stability and adaptive control techniques. As in [14], the nonlinear characteristic function of the dynamic friction model is assumed to be a function of both position and velocity, which covers a larger class of systems. Three cases are considered based on the uncertainty levels of the system: 1. unknown system parameters including all friction coefficients and the inertia parameter; 2. unknown characteristic function $\alpha(x, \dot{x})$ of the dynamic friction model; and 3. full set of unknown parameters. For Case 1, a model-based adaptive controller is presented. For Case 2, an adaptive NN controller is proposed based on a neural network parameterization of the unknown $\alpha(x, \dot{x})$. Note that in designing each of these two adaptive controllers, two nonlinear observers are used operating in parallel for the purpose of (a) estimating the unmeasurable friction state and (b) canceling the cross-coupling terms in the derivative of the Lyapunov function for closed-loop stability. For Case 3, by dividing the friction model into two portions: (i) viscous friction with unknown constant coefficient, and (ii) unknown dynamic friction which is a function of the unmeasurable internal friction state $z(t)$, and bounded by a function which is independent of $z(t)$, an adaptive NN controller is developed based on NN parameterization of the unknown dynamic friction bounding function. Using Lyapunov synthesis, adaptation algorithms are designed to achieve globally asymptotic tracking of the desired trajectory and to guarantee the boundedness of all signals in the closed loop. Both po-

sition tracking and velocity tracking are realized at the same time by the utilization of a filtered error signal.

Finally, extensive numerical comparison studies are presented. Some conclusions are drawn and comparisons made concerning applications for practical engineers.

2 Friction Models

It is well known that friction depends on both velocity and position, but its structure is not well defined, especially at low velocity. For ease of analysis and simulation, it is important to have a mathematical model of friction. A friction model should be able to accurately predict the observed friction characteristics, and be simple enough for friction compensation.

Friction is a multifaceted phenomenon, and exhibits the well-known classical Coulomb and viscous friction, nonlinearity at low velocity, and elasticity of contact surfaces. In any given circumstance, some features may dominate over others and some features may not be detectable with the available sensing technology. But all these phenomena are present all the time. The use of a more complete friction model will extend the applicability of analytical results and resolve discrepancies that arise in different investigations. While the classical friction models give only the static relationships between velocity and friction force, the most recent friction model, the so-called LuGre model, is a dynamic model with an unmeasureable internal state. In the following, we shall give a list of commonly used friction models that enable simple controller design and computer simulation.

2.1 Static Models

Static friction models refer to those models that are functions of velocity/position only, without any internal dynamics. In this subsection, we will not only list the commonly known classical static friction components, such as stiction, Coulomb etc., and we will also present a neural network friction model which is easy to use to treat the complexity and difficulty in modelling friction.

Static friction (Stiction)
At zero velocity, the static friction opposes all motion as long as the torque is smaller in magnitude than the maximum stiction force f_s, and is usually described by

$$F = \begin{cases} u, & |u| < f_s \\ f_s \delta(\dot{x}) \mathrm{sgn}(u), & |u| \geq f_s \end{cases} \tag{2.1}$$

where

$$\delta(\dot{x}) = \begin{cases} 1, & \dot{x} = 0 \\ 0, & \dot{x} \neq 0 \end{cases}, \quad \mathrm{sgn}(u) = \begin{cases} +1, & u > 0 \\ -1, & u < 0 \end{cases} \tag{2.2}$$

In actual (numerical) implementation, the impulse function can be approximated differently, such as triangular or rectangular as in Karnopp's version of stiction.

In fact, stiction is not truly a force of friction, but a force of constraint in presliding and behaves like a spring. For small motion, the elasticity of asperities suggests that the applied force is approximately proportional to the presliding displacement

$$F = f_t x \delta(\dot{x}), \tag{2.3}$$

where f_t is the tangential stiffness of the contact, x is the displacement away from equilibrium position and $\delta(\dot{x})$ is used to describe the fact that stiction occurs only when at rest. At a critical force, breakaway occurs and true sliding begins. Breakaway has been observed to occur at the order of $2-5$ microns in steel junctions and millimetre motions in robots, where the arms act as levers to amplify the micron motion at the gear teeth. Presliding displacement is of interest to the control community in extremely high precision positioning. If sensors are not sensitive enough, we are able to observe only common stiction (2.1) and Coulomb friction (2.4).

Coulomb friction (dry friction)
Independent of the area of contact, Coulomb friction always opposes relative motion and is proportional to the normal force of contact. Coulomb friction is described by

$$F = f_c \mathrm{sgn}(\dot{x}) \tag{2.4}$$

where $f_c = \mu |f_n|$ with μ being the coefficient of friction, and f_n the normal force. Constant f_c is independent of the magnitude of relative velocity.

Viscous friction
Viscous friction corresponds to the well-lubricated situation, and is proportional to velocity. It obeys the linear relationship

$$F = f_v \dot{x} \tag{2.5}$$

Drag friction
Drag friction is caused by resistance to a body moving through a fluid (e.g. wind resistance). It is proportional to the square of velocity as described by

$$F = f_d |\dot{x}| \dot{x} \tag{2.6}$$

When the speed of travel is small, this term is neglectable. This term cannot be neglected in the control of hard disk drives because of the high speed rotation of spindle motors.

Classical friction models have different combinations of static, Coulomb and viscous friction as their basic building blocks.

Exponential model

In [7], after reviewing several existing models, an exponential model incorporating Coulomb and viscous frictions is given as

$$F(\dot{x}) = f_c \text{sgn}(\dot{x}) + (f_s - f_c)e^{-(\dot{x}/\dot{x}_s)^\delta} + f_v\dot{x} \tag{2.7}$$

where $\dot{x}_s$ and δ are empirical parameters, f_c is the Coulomb friction level, f_s is the level of the stiction force and f_v is the viscous coefficient. By choosing different parameters, different frictions can be realized [4]. While the range of δ may be large, $\delta = 2$ gives the Gaussian exponential model [3] which is nearly equivalent to the Lorentzian model (2.13). Gaussian models have the following different forms:

Gaussian exponential with one break:

$$F(\dot{x}) = f_c \text{sgn}(\dot{x}) + (f_s - f_c)e^{-(\dot{x}/\dot{x}_s)^2} + f_v\dot{x} \tag{2.8}$$

Gaussian exponential with two breaks:

$$F(\dot{x}) = f_c \text{sgn}(\dot{x}) + f_v\dot{x} + f_{s_1}e^{-(\dot{x}/\dot{x}_{s_1})^2} + F_{s_2}e^{-(\dot{x}/\dot{x}_{s_2})^2} \tag{2.9}$$

Gaussian exponential with two breaks and offsets:

$$F(\dot{x}) = f_c \text{sgn}(\dot{x}) + f_v\dot{x} + f_{s_1}e^{-(\dot{x}-\dot{x}_{10})^2/\dot{x}_{s1}^2} + F_{s_2}e^{-(\dot{x}-\dot{x}_{20})^2/\dot{x}_{s2}^2} \tag{2.10}$$

where x_{s1} and x_{s2} are empirical parameters; f_{s1} and f_{s2} are static friction constants; $\dot{x}_{10}$ and $\dot{x}_{20}$ are offset points of breaks.

On the other hand, $\delta = 1$ gives Tustin's model [35] as described by

$$F(\dot{x}) = f_c \text{sgn}(\dot{x}) + (f_s - f_c)e^{-(\dot{x}/\dot{x}_s)} + f_v\dot{x} \tag{2.11}$$

Tustin's model is one of the best models describing friction force at a velocity close to zero. It includes a decaying exponential term in the friction model which explains the microscopic limit cycle behavior that, after a breakaway point at $\dot{x}$, has a negative exponential characterization. Experimental work has shown that this model can approximate real friction forces with a precision of 90% [2, 11].

Because of the nonlinearity in unknown parameter $\dot{x}_s$ in Tustin's model and the difficulty in dealing with nonlinear parameters, the following simple linear-in-the-parameters (LIP) friction model was proposed [12]:

$$F(\dot{x}) = f_c \text{sgn}(\dot{x}) + f_r\sqrt{|\dot{x}|}\text{sgn}(\dot{x}) + f_v\dot{x} \tag{2.12}$$

where constants f_i, $(i = c, r, v)$ are not unique and depend on the operating velocity. The simple LIP model has the following advantages: (i) it captures the downward bends and possible asymmetrics; (ii) the unknown parameters are linear and thus suitable for on-line identification; (iii) these parameters can accommodate parametric changes due to environmental variations; (iv)

this type of model structure reduces the possibility of friction overcompensation resulting from estimation inaccuracies caused by simplified friction model structures such as Coulomb friction and viscous friction models.

Lorentzian model
In [23], a model of the following form has been employed:

$$F(\dot{x}) = f_c \text{sgn}(\dot{x}) + (f_s - f_c)\frac{1}{1 + (\dot{x}/\dot{x}_s)^2} + f_v\dot{x} \tag{2.13}$$

which shows a systematic dependence of $\dot{x}_s$ and f_v on the lubricant and loading parameters. Similar to the case of the Gaussian model, Lorentzian models also have forms with one break, two breaks or two breaks with offsets.

Remark 2.1. Based on the above discussion, a more complete model may consist of the following components: stiction, Coulomb, viscous and drag friction, and square root friction:

$$F(x, \dot{x}) = f_t x\delta(\dot{x}) + f_c \text{sgn}(\dot{x}) + f_v\dot{x} + f_d\dot{x}|\dot{x}| + f_r\sqrt{|\dot{x}|}\text{sgn}(\dot{x}) \tag{2.14}$$

which can be conveniently expressed in LIP form as

$$F(x, \dot{x}) = S^T(x, \dot{x})P \tag{2.15}$$

where

$$S(x, \dot{x}) = [x\delta(\dot{x}), \text{sgn}(\dot{x}), \dot{x}, \dot{x}|\dot{x}|, \sqrt{|\dot{x}|}\text{sgn}(\dot{x})]^T \tag{2.16}$$

$$P = [f_t, f_c, f_v, f_d, f_r]^T \tag{2.17}$$

where $S(x, \dot{x})$ is a vector of known basis functions, and P is a vector of unknown parameters. Though the LIP form is very desirable for model-based friction compensation as will be shown later, it is in no sense complete, but is a more complete representation. If other nonlinear components, such as the nonlinear exponential term $e^{-(\dot{x}/\dot{x}_s)^\delta}$ and Lorentzian term $1/(1 + (\dot{x}/\dot{x}_s)^2)$ under the assumption of known $\dot{x}_s$ and δ, exist in the friction model, the space of the regressor function can be simply increased by including them. If $\dot{x}_s$ and δ are not known, they can be approximated using the primitives explored in [15].

Remark 2.2. It is generally considered that friction has two different manifestations, i.e. presliding friction and sliding friction [4]. In the presliding stage, which is usually in the range of less than 10^{-5}m, friction is dominated by the elasticity of the contacting asperity of surfaces as described by equation (2.3). It not only depends on both position and velocity of motion, but also exhibits nonlinear dynamic behavior such as hysteresis characteristics with respect to position and velocity as observed by many researchers. In the sliding stage, friction is dominated by lubrication of the contacting surfaces and introduces

damping into system. It is usually represented by various functions of velocity. Thus, we can conclude that *friction is continuous* though it may be highly nonlinear, and depends on both position and velocity. The discontinuities modelled by stiction (2.1) and Coulomb friction (2.4) are actually observations at the macro level. Thus, friction can be approximated by neural networks as explained below.

Neural network friction model

Neural networks offer a possible tool for nonlinear mapping approximation. Neural networks can approximate any continuous function to arbitrarily any accuracy over a compact set if the size of the network is large enough [16, 30].

Because of the complexity and difficulty in modelling friction, neural networks may be used to generate input/output maps using the property that a multilayer neural network can approximate any function, under mild assumptions, with any desired accuracy. It is well known that any sufficiently smooth function can be approximated by a suitably large network using various activation functions, $\sigma(.)$, based on the Stone–Weierstrass theorem. Typical choices for $\sigma(.)$ include the sigmoid, hyperbolic tangent, radial basis functions, etc. It has been proven that any continuous functions, not necessarily infinitely smooth, can be uniformly approximated by a linear combinations of Gaussian radial basis functions (RBF). The Gaussian RBF neural network is a particular network architecture which uses l Gaussian functions of the form

$$s_i(x, \dot{x}) = \exp\left(-\frac{(x-\mu_{1i})^2 + (\dot{x}-\mu_{2i})^2}{\sigma^2}\right), \quad i = 1, \cdots, l \tag{2.18}$$

where $x, \dot{x}$ are the input variables, σ^2 is the variance and μ_{1i}, μ_{2i} are the centres. A Gaussian RBF neural network can be mathematically expressed as

$$F_{nn}(x, \dot{x}) = W^T S(x, \dot{x}) \tag{2.19}$$

where $S(x, \dot{x}) = [s_1, s_2, ..., s_l]^T \in R^l$ is the basis function vector, and $W \in R^l$ is the corresponding weight vector. A general friction model $F(x, \dot{x})$ can then be written as

$$F(x, \dot{x}) = F_{nn}(x, \dot{x}) + \epsilon(x, \dot{x}) \tag{2.20}$$

where $F_{nn}(x, \dot{x})$ is given in (2.19), and $\epsilon(x, \dot{x})$ is the bounded neural network functional reconstruction error. If there exist integer l and constant weight W such that $\epsilon = 0$, $F(x, \dot{x})$ is said to be in the functional range of the neural network.

For ease of analysis and controller design later, we present only an LIP NN-based friction model: nonlinear multilayer NN-based friction models can

also be investigated following the method of treating multilayer NN in [26, 36]. Accordingly, we have the following LIP friction model in general form:

$$F(x, \dot{x}) = F_m(x, \dot{x}) + \epsilon(x, \dot{x}) \tag{2.21}$$

where $F_m(x, \dot{x}) = S^T(x, \dot{x})P$ is the LIP model for friction and ϵ is the residue modelling error. If $S(x, \dot{x})$ consists of the classical model basis functions listed in (2.16), P is the corresponding coefficient vector. If $S(x, \dot{x})$ is the basis function vector of the neural network model (2.19), P is the neural network weight vector.

2.2 Dynamic Models

The classical models cannot describe all the dynamic effects of friction, such as the presliding displacement, the frictional lag, the Stribeck effect, which all occur in the so-called low-velocity and pre-sliding regions. Driven by applications with high precision positioning and with low velocity tracking, there has been significant interest in dynamic friction models. In this subsection, we present two dynamic models from the literature.

Dahl model

The Dahl model was introduced in [17]. Several experiments were conducted on friction in servo systems with ball bearings. A comparatively simple model was developed to simulate systems with ball bearing friction. Let x be the displacement, F the friction force, and f_c the Coulomb friction force. Then Dahl's model has the form

$$\dot{F} = \sigma(1 - \frac{F}{f_c}\text{sgn}(\dot{x}))^{\alpha}\dot{x} \tag{2.22}$$

where σ is the stiffness coefficient and α is a parameter that determines the shape of the stress–strain curve. The value $\alpha = 1$ is most commonly used [28]. For the case $\alpha = 1$ the Dahl model (2.22) becomes

$$\dot{F} = \sigma\dot{x} - \frac{F}{f_c}|\dot{x}| \tag{2.23}$$

Introducing $F = \sigma z$, the model (2.23) can be further written as

$$\dot{z} = \dot{x} - \frac{\sigma|\dot{x}|}{f_c}z \tag{2.24}$$

$$F = \sigma z \tag{2.25}$$

Remark 2.3. The Dahl model is a generalization of ordinary Coulomb friction. It captures neither the Stribeck effect nor stiction. Recently, the Dahl model was extended to the LuGre model in [13].

LuGre model
All of the observed static and dynamic characteristics of friction can be accurately captured by the dynamic LuGre model proposed in [13]. The LuGre model considers the dynamic effects of friction to arise from the defection of bristles which model the asperities between two contacting surfaces, and is given by

$$F = \sigma_0 z + \sigma_1 \dot{z} + \sigma_2 \dot{x} \tag{2.26}$$
$$\dot{z} = \dot{x} - \alpha(\dot{x})|\dot{x}|z \tag{2.27}$$

where F is the friction force, z denotes the average deflection of the bristles, which is not measurable, $\sigma_0, \sigma_1, \sigma_2$ are friction force parameters that can be physically explained as the stiffness of bristles, damping coefficient, and viscous coefficient, and the nonlinear friction characteristic function $\alpha(\dot{x})$ is a finite positive function which can be chosen to describe different friction effects. One parameterization of $\alpha(\dot{x})$ to characterize the Stribeck effect is given in [13]

$$\alpha(\dot{x}) = \frac{\sigma_0}{f_c + (f_s - f_c)e^{-(\dot{x}/\dot{x}_s)^2}} \tag{2.28}$$

where f_c is the Coulomb friction level, f_s is the level of the stiction force and $\dot{x}_s$ is the constant Stribeck velocity.

Remark 2.4. In the above model, there are no terms which explicitly account for position dependence of the friction force. However, there may exist some applications where the function $\alpha(\cdot)$ in the LuGre model also depends on the actual position, or on a more complex combination of position and velocity. The dependency on position can also be visualized in the following scenarios as discussed in [14]. It is known that $\alpha(\cdot)$ depends on the normal force [15] between two surfaces. For a robot in operation, the normal forces on the shafts are not only functions of velocities, but also functions of positions and accelerations. In gear boxes, friction will vary as a function of the effective surface area of the gear's teeth in contact. Two–dimensional rolling and spinning friction in ball bearings causes the frictional torque to be dependent on both position and velocity. Therefore, we assume that $\alpha(x, \dot{x})$ is an upper and lower bounded positive smooth function of x and $\dot{x}$, and adopt the LuGre model in the following form:

$$F = \sigma_0 z + \sigma_1 \dot{z} + \sigma_2 \dot{x} \tag{2.29}$$
$$\dot{z} = -\alpha(x, \dot{x})|\dot{x}|z + \dot{x} \tag{2.30}$$

Assumption 2.1. *There exist positive constants α_{min} and α_m such that $0 < \alpha_{min} \leq \alpha(x, \dot{x}) \leq \alpha_m, \forall (x, \dot{x}) \in R^2$.*

Lemma 2.1. *Under Assumption 2.1, if $|z(0)| \leq 1/\alpha_{min}$ then $|z(t)| \leq 1/\alpha_{min}$, $\forall t \geq 0$ [13].*
Proof Define $V_z = \frac{1}{2}z^2$. Then the time derivative of V_z along (2.30) is

$$\dot{V}_z = z(\dot{x} - \alpha(x,\dot{x})|\dot{x}|z) = -|z||\dot{x}|(\alpha(x,\dot{x})|z| - \text{sgn}(\dot{x})\text{sgn}(z)) \tag{2.31}$$

Thus, $\dot{V}_z \leq 0$ when $|z| \geq 1/\alpha_{min}$. From $|z(0)| \leq 1/\alpha_{min}$, we always have $z(t) \leq 1/\alpha_{min}$. $\diamondsuit$

3 Adaptive Friction Compensation

3.1 Problem Statement

The servo mechanism under study is modeled as a simple mass system with dynamic friction, and is described by

$$m\ddot{x} + F = u \tag{3.1}$$

where m is the mass, x is the displacement, u is the control force, and F is the friction force.

Assumption 3.1. *States x and $\dot{x}$ are measurable for feedback controller design.*

Assumption 3.2. *The desired trajectory x_d, and its first and second derivatives $\dot{x}_d, \ddot{x}_d$ are continuous and bounded.*

The control objective is to design an adaptive controller to track the given desired trajectory. In the literature, many control techniques have been investigated for friction compensation: they include high-gain PID [5], feedforward compensation [8], robust friction compensation [9, 34], adaptive friction compensation [10, 12], neural network control [14, 21, 25]. In this section, we present adaptive controller design methods based on the LIP static friction model and the dynamic LuGre friction model.

Define the tracking errors as

$$e = x - x_d \tag{3.2}$$

$$\dot{x}_r = \dot{x}_d - \lambda e \tag{3.3}$$

$$r = \dot{e} + \lambda e \tag{3.4}$$

where $\lambda > 0$ and r is the filtered tracking error. Then the tracking error dynamics is transformed into

$$m\dot{r} = u - F - m\ddot{x}_r \tag{3.5}$$

3.2 Static Friction Model Based Adaptive Controller Design

Suppose that the friction model is given by the static LIP model (2.21), i.e.,

$$F(x,\dot{x}) = S^T(x,\dot{x})P^* + \epsilon \tag{3.6}$$

where P^* is the optimal coefficient vector and ϵ is the bounded modelling error. Then the adaptive controller can be designed based on the following description.

Substituting LIP friction model (3.6) into (3.5), we have

$$m\dot{r} = u - S^T(x,\dot{x})P^* - \epsilon - m\ddot{x}_r \tag{3.7}$$

Consider the adaptive controller given by

$$u = -k_1 r + \hat{m}\ddot{x}_r + \hat{F}_m(x,\dot{x}) - k_i \int_0^t r d\tau - u_r \tag{3.8}$$

where $k_1 > 0$, $\hat{F}_m(x,\dot{x}) = S^T(x,\dot{x})\hat{P}$, and u_r is a robust control term for suppressing any modelling uncertainty. For now, let us consider $u_r = k_2 \mathrm{sgn}(r)$ with $k_2 \geq \epsilon$.

Substituting (3.8) into (3.7), we have the closed-loop error dynamics

$$\begin{aligned} m\dot{r} &= -k_1 r - u_r - k_i \int_0^t r d\tau - \tilde{m}\ddot{x}_r - S^T(x,\dot{x})\tilde{P} + \epsilon \\ &= -k_1 r - u_r - k_i \int_0^t r d\tau - \psi^T \tilde{\theta} + \epsilon \end{aligned} \tag{3.9}$$

where $(\tilde{*}) = (*) - (\hat{*})$, $\psi^T = [\ddot{x}_r, S^T(x,\dot{x})]$ and $\tilde{\theta} = [\tilde{m}, \tilde{P}]^T$.

The closed-loop stability properties are then summarized in Theorem 3.1.

Theorem 3.1. *Consider the closed–loop system consisting of (3.1) with LIP static friction given by (2.21) and adaptive controller (3.8). If the parameters $\hat{\theta}$ are updated by*

$$\dot{\hat{\theta}} = -\Gamma \psi r \tag{3.10}$$

where $\Gamma^T = \Gamma > 0$, then the tracking error converges to zero and all the signals in the closed loop are bounded.

Proof Consider the Lyapunov function candidate

$$V = \frac{1}{2} m r^2 + \frac{1}{2}\tilde{\theta}^T \Gamma^{-1} \tilde{\theta} + \frac{1}{2} k_i (\int_0^t r d\tau)^2 \tag{3.11}$$

Its time derivative is given by

$$\dot{V} = m r \dot{r} + \tilde{\theta}^T \Gamma^{-1} \dot{\tilde{\theta}} + r k_i \int_0^t r d\tau \tag{3.12}$$

Substituting (3.9) into (3.12) leads to

$$\begin{aligned} \dot{V} &= r(\epsilon - \psi^T \tilde{\theta} - k_1 r - u_r) + \tilde{\theta}^T \Gamma^{-1} \dot{\tilde{\theta}} \\ &= -k_1 r^2 + r(\epsilon - u_r) - r\psi^T \tilde{\theta} + \tilde{\theta}^T \Gamma^{-1} \dot{\tilde{\theta}} \end{aligned} \tag{3.13}$$

Noting that $(\dot{\tilde{*}}) = -(\dot{\hat{*}})$ and substituting adaptation law (3.10) into (3.13), we have

$$\dot{V} = -k_1 r^2 + r(\epsilon - u_r) \tag{3.14}$$

Since $u_r = k_2 \text{sgn}(r)$ and $k_2 \geq |\epsilon|$, we have $\dot{V} = -k_1 r^2 \leq 0$. It follows that $0 \leq V(t) \leq V(0), \forall t \geq 0$. Hence $V(t) \in L_\infty$, which implies that $\tilde{\theta}$ is bounded. In other words, $\hat{\theta}$ is bounded for θ constant although unknown. Since $r \in L_2$, $e \in L_2 \cap L_\infty$, e is continuous and $e \to 0$ as $t \to \infty$, and $\dot{e} \in L_2$. By noting that $r \in L_2$, x_d, $\dot{x}_d$, $\ddot{x}_d \in L_\infty$, and ψ is of bounded functions, it is concluded that $\dot{r} \in L_\infty$ from equation (3.9). Using the fact that $r \in L_2$ and $\dot{r} \in L_\infty$, thus $r \to 0$ as $t \to \infty$. Hence $\dot{e} \to 0$ as $t \to \infty$. $\diamondsuit$

With regard to the implementation issues, we make the following remarks.

Remark 3.1. The presence of sgn$(\cdot)$ function in the sliding mode control inevitably introduces chattering, which is undesirable as it may excite mechanical resonance and cause mechanical wear and tear. To alleviate this problem, many approximation mechanisms have been used, such as boundary layer, saturation functions [20], and hyperbolic tangent function, tanh$(\cdot)$, which has the following property [31]

$$0 \leq |\alpha| - \alpha \tanh(\frac{\alpha}{\varepsilon}) \leq 0.2785\varepsilon, \quad \forall \alpha \in R \tag{3.15}$$

By smoothing the sgn$(\cdot)$ function, although asymptotic stability can no longer be guaranteed, the closed-loop system is still stable but with a small residue error. For example, if $u_r = k_2 \tanh(r/\epsilon_r)$, where $\epsilon_r > 0$ is a constant, and $k_2 \geq |\epsilon|$, then (3.14) becomes

$$\begin{aligned} \dot{V} &= -k_1 r^2 + r(\epsilon - u_r) \\ &\leq -k_1 r^2 + |r||\epsilon| - r k_2 \tanh(\frac{r}{\epsilon_r}) \\ &\leq -k_1 r^2 + |r| k_2 - r k_2 \tanh(\frac{r}{\epsilon_r}) \end{aligned} \tag{3.16}$$

Using (3.15), (3.16) can be further simplified to

$$\dot{V} \leq -k_1 r^2 + 0.2785 \epsilon_r k_2 \tag{3.17}$$

Obviously, $\dot{V} \leq 0$ whenever r is outside the compact set

$$D = \{r | r^2 \leq \frac{0.2785 \epsilon_r k_2}{k_1}\} \tag{3.18}$$

Thus, we can conclude that the closed-loop system is stable and the tracking error will converge to a small neighborhood of zero, whose size is adjustable by the design parameters k_1 and ϵ_r.

It should be mentioned that these modification may cause the estimated parameters to grow unboundedly because asymptotic tracking cannot be guaranteed. To deal with this problem, the σ-modification scheme or e-modification, and among others [24], can be used to modify the adaptive laws to guarantee the robustness of the closed-loop system in the presence of approximation errors. For example, $\hat{\theta}$ can be adaptively tuned by

$$\dot{\hat{\theta}} = -\Gamma\phi r - \sigma\hat{\theta} \tag{3.19}$$

where $\sigma > 0$. The additional σ term in (3.19) ensures the boundedness of $\hat{\theta}$ when the system is subject to bounded disturbances without any additional prior information about the plant. The drawback is that tracking errors may only be made arbitrarily small rather than zero.

Remark 3.2. In this paper, only Gaussian RBF neural networks are discussed. If fact, other neural networks can also be used without any difficulty, and include other RBF neural networks, high order neural networks, and multilayer neural networks [26, 36].

3.3 LuGre Friction Model Based Adaptive Controller Design

In this subsection, the dynamic LuGre friction model based adaptive controller design will be presented. For the dynamic friction model (2.29-2.30), the uncertainties can be divided into two groups: (i) the unknown nonlinear friction characteristic function $\alpha(x, \dot{x})$; and (ii) the friction parameters σ_0, σ_1 and σ_2 which are assumed to change nonuniformly. Since $\alpha(x, \dot{x})$ is very hard to model, neural networks (NN) offer a possible tool for nonlinear mapping approximation. For simplicity, RBF NNs shall be used for function approximation though other neural networks can also be used without any difficulty.

In the following, we shall present three novel adaptive compensation schemes for dynamic friction under different situations: (i) unknown friction parameters $\sigma_0, \sigma_1, \sigma_2$ and unknown inertia parameter m; (ii) unknown nonlinear function $\alpha(x, \dot{x})$; and (iii) unknown full set of related parameters and nonlinear function.

Substituting friction dynamics (2.29) into (3.5), we have the following tracking error dynamics

$$m\dot{r} = u - (\sigma_1 + \sigma_2)\dot{x} - \sigma_0 z + \alpha(x, \dot{x})\sigma_1|\dot{x}|z - m\ddot{x}_r \tag{3.20}$$

3.3.1 Controller design for unknown system parameters

Firstly, let us investigate the case where the system parameter m and dynamic friction parameters $\sigma_0, \sigma_1, \sigma_2$ are unknown while nonlinear function $\alpha(x, \dot{x})$ is known.

Motivated by the work in [32], the following dual-observer is adopted to estimate the unmeasurable friction state z:

$$\dot{\hat{z}}_0 = \dot{x} - \alpha(x, \dot{x})|\dot{x}|\hat{z}_0 - r \tag{3.21}$$

$$\dot{\hat{z}}_1 = \dot{x} - \alpha(x, \dot{x})|\dot{x}|\hat{z}_1 + \alpha(x, \dot{x})|\dot{x}|r \tag{3.22}$$

where $\hat{z}_0$ and $\hat{z}_1$ are estimates of the friction state z. Combining with equation (2.30), the corresponding observation errors are given by

$$\dot{\tilde{z}}_0 = -\alpha(x,\dot{x})|\dot{x}|\tilde{z}_0 + r \tag{3.23}$$
$$\dot{\tilde{z}}_1 = -\alpha(x,\dot{x})|\dot{x}|\tilde{z}_1 - \alpha(x,\dot{x})|\dot{x}|r \tag{3.24}$$

where $\tilde{z}_0 = z - \hat{z}_0$ and $\tilde{z}_1 = z - \hat{z}_1$.

Remark 3.3. The two friction state observers are introduced here for different purposes. Observers (3.21) and (3.22) driven by $-r$ and $\alpha(x,\dot{x})|\dot{x}|r$ are introduced to cancel the cross-coupling terms $-\sigma_0 r\tilde{z}_0$ and $\alpha(x,\dot{x})\sigma_1|\dot{x}|r\tilde{z}_1$ respectively in (3.34), the derivative of the Lyapunov function candidate, for closed-loop stability. Due to the fact that the filtered tracking error r asymptotically converges to zero as will be proven in Theorem 3.2, it is then expected that the output $\hat{z}_0$ of observer (3.21) will reveal the actual friction state z. Though we can prove that $\hat{z}_1$ is bounded in Theorem 3.2, we could not claim that it is small. In fact, since $\alpha(x,\dot{x})$ can take a very large value, a small error in r will result in a large driving value in (3.24), accordingly $\hat{z}_1$ may become very large in comparison with z as will be verified by a simulation study later.

Let $\hat{\sigma}_0, \hat{\sigma}_1, \hat{\sigma}_2$ and $\hat{m}$ be the estimates of unknown friction parameters $\sigma_0, \sigma_1, \sigma_2$ and inertia parameter m. Consider the adaptive controller u given by

$$u = -c_1 r + \hat{\sigma}_1\dot{x} + \hat{\sigma}_2\dot{x} + \hat{\sigma}_0\hat{z}_0 - \alpha(x,\dot{x})\hat{\sigma}_1|\dot{x}|\hat{z}_1 + \hat{m}\ddot{x}_r \tag{3.25}$$

where c_1 is a positive design constant.

Substituting (3.25) into (3.20), we have the closed-loop error dynamics

$$\begin{aligned} m\dot{r} = {} & -c_1 r - \tilde{\sigma}_1\dot{x} - \tilde{\sigma}_2\dot{x} - \sigma_0\tilde{z}_0 - \tilde{\sigma}_0\hat{z}_0 + \alpha(x,\dot{x})\sigma_1|\dot{x}|\tilde{z}_1 \\ & + \alpha(x,\dot{x})\tilde{\sigma}_1|\dot{x}|\hat{z}_1 - \tilde{m}\ddot{x}_r \end{aligned} \tag{3.26}$$

where $(\tilde{*}) = (*) - (\hat{*})$ are the parameter estimates errors.

Theorem 3.2. *Consider the closed system consisting of system (3.1) with dynamic friction given by (2.29) and (2.30), adaptive controller (3.25) and dual-observer given by (3.21) and (3.22). If the parameters $\hat{\sigma}_0, \hat{\sigma}_1, \hat{\sigma}_2$ and $\hat{m}$ are updated by*

$$\dot{\hat{\sigma}}_0 = -\eta_0\hat{z}_0 r \tag{3.27}$$
$$\dot{\hat{\sigma}}_1 = -\eta_1(r\dot{x} - \alpha(x,\dot{x})|\dot{x}|r\hat{z}_1) \tag{3.28}$$
$$\dot{\hat{\sigma}}_2 = -\eta_2\dot{x}r \tag{3.29}$$
$$\dot{\hat{m}} = -\eta_m\ddot{x}_r r \tag{3.30}$$

where η_0, η_1, η_2 and η_m are positive constants, then the tracking error converges to zero and all the signals in the closed loop are bounded.

Proof Consider the Lyapunov function candidate

$$V = \frac{1}{2}mr^2 + \frac{1}{2}\sigma_0\tilde{z}_0^2 + \frac{1}{2}\sigma_1\tilde{z}_1^2 + \frac{1}{2\eta_0}\tilde{\sigma}_0^2 + \frac{1}{2\eta_1}\tilde{\sigma}_1^2 + \frac{1}{2\eta_2}\tilde{\sigma}_2^2 + \frac{1}{2\eta_m}\tilde{m}^2 \tag{3.31}$$

where $\eta_0, \eta_1, \eta_2, \eta_m$ are positive design constants.

Evaluating the time derivative of V along (3.26), we obtain

$$\begin{aligned}\dot{V} &= mr\dot{r} + \sigma_0\tilde{z}_0\dot{\tilde{z}}_0 + \sigma_1\tilde{z}_1\dot{\tilde{z}}_1 + \frac{1}{\eta_0}\tilde{\sigma}_0\dot{\tilde{\sigma}}_0 + \frac{1}{\eta_1}\tilde{\sigma}_1\dot{\tilde{\sigma}}_1 + \frac{1}{\eta_2}\tilde{\sigma}_2\dot{\tilde{\sigma}}_2 + \frac{1}{\eta_m}\tilde{m}\dot{\tilde{m}} \\ &= -c_1r^2 - \tilde{\sigma}_1 r\dot{x} - \tilde{\sigma}_2 r\dot{x} - \sigma_0 r\tilde{z}_0 - \tilde{\sigma}_0 r\hat{z}_0 \\ &\quad +\alpha(x,\dot{x})\sigma_1|\dot{x}|r\tilde{z}_1 + \alpha(x,\dot{x})\tilde{\sigma}_1|\dot{x}|r\hat{z}_1 - \tilde{m}r\ddot{x}_r + \sigma_0\tilde{z}_0\dot{\tilde{z}}_0 \\ &\quad +\sigma_1\tilde{z}_1\dot{\tilde{z}}_1 + \frac{1}{\eta_0}\tilde{\sigma}_0\dot{\tilde{\sigma}}_0 + \frac{1}{\eta_1}\tilde{\sigma}_1\dot{\tilde{\sigma}}_1 + \frac{1}{\eta_2}\tilde{\sigma}_2\dot{\tilde{\sigma}}_2 + \frac{1}{\eta_m}\tilde{m}\dot{\tilde{m}} \qquad (3.32)\end{aligned}$$

Re-arranging the related items in (3.32), we have

$$\begin{aligned}\dot{V} &= -c_1r^2 - \tilde{\sigma}_0(r\hat{z}_0 - \frac{1}{\eta_0}\dot{\tilde{\sigma}}_0) - \tilde{\sigma}_1(r\dot{x} - \alpha(x,\dot{x})|\dot{x}|r\hat{z}_1 - \frac{1}{\eta_1}\dot{\tilde{\sigma}}_1) \\ &\quad -\tilde{\sigma}_2(r\dot{x} - \frac{1}{\eta_2}\dot{\tilde{\sigma}}_2) - \tilde{m}(r\ddot{x}_r - \frac{1}{\eta_m}\dot{\tilde{m}}) - \sigma_0 r\tilde{z}_0 \\ &\quad +\alpha(x,\dot{x})\sigma_1|\dot{x}|r\tilde{z}_1 + \sigma_0\tilde{z}_0\dot{\tilde{z}}_0 + \sigma_1\tilde{z}_1\dot{\tilde{z}}_1 \qquad (3.33)\end{aligned}$$

Noting that $(\dot{\tilde{*}}) = -(\dot{\hat{*}})$ and substituting adaptation laws (3.27-3.30) into (3.33) yields

$$\dot{V} = -c_1r^2 - \sigma_0 r\tilde{z}_0 + \alpha(x,\dot{x})\sigma_1|\dot{x}|r\tilde{z}_1 + \sigma_0\tilde{z}_0\dot{\tilde{z}}_0 + \sigma_1\tilde{z}_1\dot{\tilde{z}}_1 \qquad (3.34)$$

In order to cancel the terms $-\sigma_0 r\tilde{z}_0$ and $\alpha(x,\dot{x})\sigma_1|\dot{x}|r\tilde{z}_1$ in (3.34), substituting the observer error dynamics (3.23) and (3.24) into (3.34), we obtain

$$\begin{aligned}\dot{V} &= -c_1r^2 - \sigma_0 r\tilde{z}_0 + \alpha(x,\dot{x})\sigma_1|\dot{x}|r\tilde{z}_1 + \sigma_0\tilde{z}_0(-\alpha(x,\dot{x})|\dot{x}|\tilde{z}_0 + r) \\ &\quad +\sigma_1\tilde{z}_1(-\alpha(x,\dot{x})|\dot{x}|\tilde{z}_1 - \alpha(x,\dot{x})|\dot{x}|r) \\ &= -c_1r^2 - \sigma_0\alpha(x,\dot{x})|\dot{x}|\tilde{z}_0^2 - \sigma_1\alpha(x,\dot{x})|\dot{x}|\tilde{z}_1^2 \qquad (3.35)\end{aligned}$$

Obviously, the following inequality holds

$$\dot{V} = -c_1r^2 - \sigma_0\alpha(x,\dot{x})|\dot{x}|\tilde{z}_0^2 - \sigma_1\alpha(x,\dot{x})|\dot{x}|\tilde{z}_1^2 \leq 0 \qquad (3.36)$$

for c_1, σ_0, σ_1 and $\alpha(\cdot)$ are positive.

From the definition of Lyapunov function V in (3.31) and $\dot{V} \leq 0$, the global uniform boundedness of the tracking error r, the observer errors $\tilde{z}_0, \tilde{z}_1$, and the parameter estimation errors $\tilde{\sigma}_0, \tilde{\sigma}_1, \tilde{\sigma}_2, \tilde{m}$ are guaranteed. Obviously, the estimates $\hat{\sigma}_0, \hat{\sigma}_1, \hat{\sigma}_2$ and $\hat{m}$ are bounded. From the definition of r and Assumption 3.2, it can also be concluded that the tracking error e is bounded. The boundedness of the control u is apparent from (3.25). Since $r \in L_2, e \in L_2 \cap L_\infty$, e is continuous and $e \to 0$ as $t \to \infty$, and $\dot{e} \in L_2$. By noting that $r \in L_2$ and $x_d, \dot{x}_d, \ddot{x}_d \in L_\infty$, it is concluded that $\dot{r} \in L_\infty$ from equation (3.26). Using the fact that $r \in L_2$ and $\dot{r} \in L_\infty$, thus $r \to 0$ as $t \to 0$. Hence $\dot{e} \to 0$ as $t \to 0$. $\diamondsuit$

3.3.2 Controller design for unknown $\alpha(x, \dot{x})$

Assuming that the parameters $m, \sigma_0, \sigma_1, \sigma_2$ are known while the nonlinear function $\alpha(x, \dot{x})$ is unknown. Note that the parameterization given in (2.28) is not exclusive. Rather than finding another analytical description of $\alpha(x, \dot{x})$ for better or for worse, we shall use the RBF NN $\hat{\alpha}(x, \dot{x}) = W^T S(x, \dot{x})$ to approximate the unknown $\alpha(x, \dot{x})$. Since $\alpha(x, \dot{x})$ is a continuous function, according to the general approximation ability of neural networks [20], the following function approximation holds over a compact set $\Omega \subset R^2$

$$\alpha(x, \dot{x}) = W^{*T} S(x, \dot{x}) + \epsilon, \ \forall (x, \dot{x}) \in \Omega \tag{3.37}$$

where W^* is the optimal weight vector.

Assumption 3.3 *The neural network approximation error ϵ is bounded over the compact set Ω, i.e., $|\epsilon| \leq \epsilon_b$, where ϵ_b is a small positive constant.*

In this case, since $\alpha(x, \dot{x})$ is unknown, observers (3.21) and (3.22) cannot be used. Therefore, an auxiliary variable $\delta = z + \frac{m}{\sigma_1} r$ is defined to implement the estimate for the internal friction state z. Its derivative is then given by

$$\dot{\delta} = \dot{z} + \frac{m}{\sigma_1} \dot{r} = (\dot{x} - \alpha(x, \dot{x}) |\dot{x}| z) + \frac{m}{\sigma_1} \dot{r} \tag{3.38}$$

Substituting (3.20) and $z = \delta - \frac{m}{\sigma_1} r$ into (3.38) yields

$$\dot{\delta} = \dot{x} - \frac{\sigma_0}{\sigma_1} \delta + \frac{m \sigma_0}{\sigma_1^2} r + \frac{1}{\sigma_1} (u - (\sigma_1 + \sigma_2) \dot{x} - m \ddot{x}_r) \tag{3.39}$$

To estimate the unmeasurable friction state δ, consider the following dual-observer

$$\dot{\hat{\delta}}_1 = \dot{x} - \frac{\sigma_0}{\sigma_1} \hat{\delta}_1 + \frac{m \sigma_0}{\sigma_1^2} r + \frac{1}{\sigma_1} (u - (\sigma_1 + \sigma_2) \dot{x} - m \ddot{x}_r) - r \tag{3.40}$$

$$\dot{\hat{\delta}}_2 = \dot{x} - \frac{\sigma_0}{\sigma_1} \hat{\delta}_2 + \frac{m \sigma_0}{\sigma_1^2} r + \frac{1}{\sigma_1} (u - (\sigma_1 + \sigma_2) \dot{x} - m \ddot{x}_r) + \sigma_1 r \dot{x} \tag{3.41}$$

where $\hat{\delta}_1$ and $\hat{\delta}_2$ are the estimates of friction state δ. Combining (3.39) with the dual–observer, we can obtain the internal friction state error dynamics as follows:

$$\dot{\tilde{\delta}}_1 = -\frac{\sigma_0}{\sigma_1} \tilde{\delta}_1 + r \tag{3.42}$$

$$\dot{\tilde{\delta}}_2 = -\frac{\sigma_0}{\sigma_2} \tilde{\delta}_2 - \sigma_1 r \dot{x} \tag{3.43}$$

where $\tilde{\delta}_1 = \delta - \hat{\delta}_1$ and $\tilde{\delta}_2 = \delta - \hat{\delta}_2$.

Remark 3.4. Similarly, two friction state observers are introduced here for different purposes. Observers (3.40) and (3.41) driven by $-r$ and $\sigma_1 r \dot{x}$ are introduced to cancel the cross-coupling terms $-\sigma_0 r \tilde{\delta}_1$ and $\sigma_1 r \alpha(x, \dot{x}) |\dot{x}| \tilde{\delta}_2$ respectively in (3.50), the derivative of the Lyapunov function candidate,

for closed-loop stability. Due to the fact that the filtered tracking error r asymptotically converges to zero as will be proven in Theorem 3.3, it is then expected that the output $\hat{\delta}_1$ of observer (3.40) will reveal the actual friction state δ. Though we can prove that $\hat{\delta}_2$ is bounded in Theorem 3.3, we could not claim that it is small. In fact, since σ_1 can take a large value, a small error in r will result in a large driving value in (3.43), accordingly $\hat{\delta}_2$ may become large in comparison with δ as will be verified by a simulation study later.

Using $z = \delta - \frac{m}{\sigma_1} r$, equation (3.20) can be rewritten as

$$\begin{aligned} m\dot{r} &= -\sigma_0 \delta + \sigma_1 \alpha(x, \dot{x}) |\dot{x}| \delta + \frac{m\sigma_0}{\sigma_1} r - m\alpha(x, \dot{x}) |\dot{x}| r \\ &\quad + u - (\sigma_1 + \sigma_2)\dot{x} - m\ddot{x}_r \end{aligned} \tag{3.44}$$

Consider the control law

$$u = (\sigma_1 + \sigma_2)\dot{x} + m\ddot{x}_r + u_{ar} \tag{3.45}$$

where u_{ar} is the adaptive robust control term given by

$$\begin{aligned} u_{ar} &= -c_1 r + \sigma_0 \hat{\delta}_1 - \sigma_1 \hat{\alpha}(x, \dot{x}) |\dot{x}| \hat{\delta}_2 - \frac{m\sigma_0}{\sigma_1} r - \frac{\sigma_1^2 \sigma_2 \alpha_m r \dot{x}^2}{\sigma_0} \\ &\quad - k\sigma_1 |\dot{x}| |\hat{\delta}_2| \mathrm{sgn}(r) \end{aligned} \tag{3.46}$$

with $\hat{\alpha}(x, \dot{x}) = W^T S(x, \dot{x})$, constants $c_1 > 0$ and $k \geq \epsilon_b$.

Substituting (3.46) into (3.44), we have

$$\begin{aligned} m\dot{r} &= -c_1 r - \sigma_0 \tilde{\delta}_1 + \sigma_1 \alpha(x, \dot{x}) |\dot{x}| \tilde{\delta}_2 + \sigma_1 (\tilde{W}^T S(x, \dot{x}) + \epsilon) |\dot{x}| \hat{\delta}_2 \\ &\quad - m\alpha(x, \dot{x}) |\dot{x}| r - \frac{\sigma_1^2 \sigma_2 \alpha_m r \dot{x}^2}{\sigma_0} - k\sigma_1 |\dot{x}| |\hat{\delta}_2| \mathrm{sgn}(r) \end{aligned} \tag{3.47}$$

where $\tilde{W} = W^* - W$.

Remark 3.5. The presence of k is for robust closed-loop stability because of the existence of $\epsilon \neq 0$. The particlar choice of the dynamic gain, $k\sigma_1 |\hat{\delta}_2| |\dot{x}|$, has the following advantages: (i) the value of k needs only to be large enough to suppress the bounded approximation error ϵ, and (ii) the gain is a function of $|\hat{\delta}_2| |\dot{x}|$ so that it is zero whenever $|\hat{\delta}_2| = 0$ and/or $|\dot{x}| = 0$, and decreases as $|\hat{\delta}_2| |\dot{x}|$ diminishes.

Theorem 3.3. *Consider the closed-loop system consisting of system (3.1) with dynamic friction given by (2.29) and (2.30), adaptive controller (3.45) and (3.46), and dual-observer (3.40) and (3.41). If the weights of NN approximation to $\alpha(x, \dot{x})$ are updated by*

$$\dot{W} = \Gamma S(x, \dot{x}) \sigma_1 |\dot{x}| \hat{\delta}_2 r \tag{3.48}$$

where $\Gamma = \Gamma^T > 0$ is a dimensionally compatible constant matrix, then the tracking error converges to zero and all the signals in the closed loop are bounded.

Proof Consider the Lyapunov function candidate

$$V = \frac{1}{2}mr^2 + \frac{1}{2}\sigma_0\tilde{\delta}_1^2 + \frac{1}{2}\alpha_m\tilde{\delta}_2^2 + \frac{1}{2}\tilde{W}^T\Gamma^{-1}\tilde{W} \tag{3.49}$$

The time derivative of V along (3.47) is

$$\begin{aligned}
\dot{V} &= mr\dot{r} + \sigma_0\tilde{\delta}_1\dot{\tilde{\delta}}_1 + \alpha_m\tilde{\delta}_2\dot{\tilde{\delta}}_2 + \tilde{W}\Gamma^{-1}\dot{\tilde{W}} \\
&= -c_1r^2 - \sigma_0 r\tilde{\delta}_1 + \sigma_1 r\alpha(x,\dot{x})|\dot{x}|\tilde{\delta}_2 + \sigma_1 r(\tilde{W}^T S(x,\dot{x}) + \epsilon)|\dot{x}|\hat{\delta}_2 \\
&\quad -m\alpha(x,\dot{x})|\dot{x}|r^2 - \frac{\sigma_1^2\sigma_2\alpha_m r^2\dot{x}^2}{\sigma_0} - k\sigma_1|\dot{x}||\hat{\delta}_2|r\mathrm{sgn}(r) + \sigma_0\tilde{\delta}_1\dot{\tilde{\delta}}_1 \\
&\quad +\alpha_m\tilde{\delta}_2\dot{\tilde{\delta}}_2 + \tilde{W}^T\Gamma^{-1}\dot{\tilde{W}}
\end{aligned} \tag{3.50}$$

Substituting the observer error dynamics (3.42) and (3.43) into (3.50) and noting $\alpha(x,\dot{x}) \le \alpha_m$, we have

$$\begin{aligned}
\dot{V} &= -c_1r^2 - m\alpha(x,\dot{x})|\dot{x}|r^2 - \frac{\sigma_0^2}{\sigma_1}\tilde{\delta}_1^2 - \frac{\alpha_m\sigma_0}{\sigma_2}\tilde{\delta}_2^2 + \sigma_1\alpha(x,\dot{x})r|\dot{x}|\tilde{\delta}_2 \\
&\quad -\sigma_1\alpha_m r\dot{x}\tilde{\delta}_2 - \frac{\sigma_1^2\sigma_2\alpha_m r^2\dot{x}^2}{\sigma_0} + \sigma_1\epsilon|\dot{x}|r\hat{\delta}_2 - k\sigma_1|\dot{x}||\hat{\delta}_2|r\mathrm{sgn}(r) \\
&\quad +\tilde{W}^T(\sigma_1 rS(x,\dot{x})|\dot{x}|\hat{\delta}_2 + \Gamma^{-1}\dot{\tilde{W}}) \\
&\le -c_1r^2 - m\alpha(x,\dot{x})|\dot{x}|r^2 - \frac{\sigma_0^2}{\sigma_1}\tilde{\delta}_1^2 - \frac{\alpha_m\sigma_0}{\sigma_2}\tilde{\delta}_2^2 \\
&\quad +2\sigma_1\alpha_m|r||\dot{x}||\tilde{\delta}_2| - \frac{\sigma_1^2\sigma_2\alpha_m r^2\dot{x}^2}{\sigma_0} + \sigma_1|\epsilon||\dot{x}||r||\hat{\delta}_2| \\
&\quad -k\sigma_1|\dot{x}||\hat{\delta}_2|r\mathrm{sgn}(r) + \tilde{W}^T(\sigma_1 rS(x,\dot{x})|\dot{x}|\hat{\delta}_2 + \Gamma^{-1}\dot{\tilde{W}})
\end{aligned} \tag{3.51}$$

Using the fact that

$$\begin{aligned}
2\sigma_1\alpha_m|r||\dot{x}||\tilde{\delta}_2| &\le \frac{(2\sigma_1\alpha_m|r||\dot{x}|)^2}{4\alpha_m\sigma_0/\sigma_2} + \frac{\alpha_m\sigma_0}{\sigma_2}\tilde{\delta}_2^2 \\
&= \frac{\sigma_1^2\sigma_2\alpha_m r^2\dot{x}^2}{\sigma_0} + \frac{\alpha_m\sigma_0}{\sigma_2}\tilde{\delta}_2^2
\end{aligned} \tag{3.52}$$

and substituting adaptation law (3.48) into (3.51), and noting $|\epsilon| \le k$, we have the following inequality

$$\dot{V} \le -c_1r^2 - m\alpha(x,\dot{x})|\dot{x}|r^2 - \frac{\sigma_0^2}{\sigma_1}\tilde{\delta}_1^2 \le 0 \tag{3.53}$$

for c_1, σ_0, σ_1 and $\alpha(\cdot)$ are positive.

From the definition of Lyapunov function V in (3.49) and $\dot{V} \leq 0$, the global uniform boundedness of the tracking error r, the observer errors $\tilde{\delta}_1, \tilde{\delta}_2$, and the parameter estimation errors $\tilde{W}$ are guaranteed. From the definition of r and Assumption 3.2, it can also be concluded that the tracking error e is bounded. The boundedness of control u is apparent from (3.45).

Since $r \in L_2, e \in L_2 \cap L_\infty$, e is continuous and $e \to 0$ as $t \to \infty$, and $\dot{e} \in L_2$. By noting that $r \in L_2$ and $x_d, \dot{x}_d, \ddot{x}_d \in L_\infty$, it is concluded that $\dot{r} \in L_\infty$ from equation (3.47). Using the fact that $r \in L_2$ and $\dot{r} \in L_\infty$, thus $r \to 0$ as $t \to 0$. Hence $\dot{e} \to 0$ as $t \to 0$. $\diamondsuit$

Remark 3.6. It is well known that when using dynamic friction models, controller design becomes difficult because (i) the friction parameters appear in a nonlinear fashion, and (ii) the systems's internal state z, which depends on the unknown parameters, is not measurable. One of the main contributions here is the introduction of an easily implementable approach to cope with the completely unknown $\alpha(x, \dot{x})$ by using the concept of dual-observer and neural network parameterization.

3.3.3 Controller design for full set of unknown parameters

In practice, friction compensation becomes more challenging when the related parameters and functions of the system are unknown. In [21], neural network parameterization was presented for the completely unknown static friction model. Through intensive computer simulation study, it was found that the proposed controller is effective in handling dynamic friction. By separating the dynamic friction into a static function of velocity with a dynamic perturbation in friction, and using a convex/concave parameterization, an adaptive nonlinear control scheme was presented in [27] to achieve dynamic friction compensation. In [29], using the boundedness property of the internal friction state $z(t)$, a simple linearly parameterized friction model was first presented and then adaptive control was developed based on the simplified model. In this section, motivated by the work in [21, 29], the dynamic friction is first separated into two parts: (i) the viscous friction with unknown constant coefficient, and (ii) the unknown dynamic friction which is a function of the unmeasurable internal friction state $z(t)$ and is bounded by a function which is independent of $z(t)$. Then an RBF NN is applied to approximate this unknown bounding function. Based on Lyapunov synthesis, adaptation algorithms for both the NN weights and the unknown system and friction parameters are presented.

In particular, the dynamic friction (2.29) can be further written as

$$\begin{aligned} F &= \sigma_1 \dot{x} + \sigma_2 \dot{x} + \sigma_0 z - \sigma_1 \alpha(x, \dot{x}) |\dot{x}| z \\ &= \theta \dot{x} + F_z(x, \dot{x}, z) \end{aligned} \tag{3.54}$$

where $\theta = \sigma_1 + \sigma_2$, $\theta \dot{x}$ represents the viscous friction force and $F_z(x, \dot{x}, z) = \sigma_0 z - \sigma_1 \alpha(x, \dot{x}) |\dot{x}| z$ is the dynamic friction force which depends on z.

From Lemma 2.1, we know that F_z is bounded by

$$|F_z(x,\dot{x},z)| = |(\sigma_0 - \sigma_1\alpha(x,\dot{x}))||z(t)| \leq \frac{\sigma_0 + \sigma_1\alpha(x,\dot{x})}{\alpha_{min}} = F_{zm}(x,\dot{x}) \quad (3.55)$$

where $F_{zm}(x,\dot{x})$ is the bounding function of $F_z(x,\dot{x},z)$ and is independent of the unmeasurable internal friction state z. An RBF NN can be applied to approximate $F_{zm}(x,\dot{x})$, and similarly there exists the following function approximation

$$F_{zm}(x,\dot{x}) = W^{*T}S(x,\dot{x}) + \epsilon \quad (3.56)$$

with W^* being the optimal weight vector, and the NN approximation error ϵ being bounded by a small positive constant ϵ_d, i.e., $|\epsilon| \leq \epsilon_d$.

System tracking error dynamics (3.20) can be rewritten as

$$\begin{aligned} m\dot{r} &= u - (\sigma_1 + \sigma_2)\dot{x} - \sigma_0 z + \alpha(x,\dot{x})\sigma_1|\dot{x}|z - m\ddot{x}_r \\ &= u - \theta\dot{x} - F_z(x,\dot{x},z) - m\ddot{x}_r \end{aligned} \quad (3.57)$$

Consider the following controller

$$u = -c_1 r + \hat{\theta}\dot{x} + \hat{m}\ddot{x}_r - \hat{F}_{zm}(x,\dot{x})\text{sgn}(r) - k\text{sgn}(r) \quad (3.58)$$

where constant $c_1 > 0$, $\hat{\theta}$ and $\hat{m}$ are the estimates of unknown θ and m respectively, $\hat{F}_{zm}(x,\dot{x}) = W^T S(x,\dot{x})$ is the RBF NN approximation of function bound $F_{zm}(x,\dot{x})$, and $k > \epsilon_d$.

Substituting (3.58) into (3.57) yields

$$m\dot{r} = -c_1 r - \tilde{\theta}\dot{x} - \tilde{m}\ddot{x}_r - \hat{F}_{zm}(x,\dot{x})\text{sgn}(r) - k\text{sgn}(r) - F_z(x,\dot{x},z) \quad (3.59)$$

where $(\tilde{*}) = (*) - (\hat{*})$ denotes the unknown parameter estimation errors.

Adding and subtracting $F_{zm}(x,\dot{x})\text{sgn}(r)$ in (3.59) and noting equation (3.56), we have

$$\begin{aligned} m\dot{r} &= -c_1 r - \tilde{\theta}\dot{x} - \tilde{m}\ddot{x}_r + (\tilde{W}^T S(x,\dot{x}) + \epsilon)\text{sgn}(r) - F_z(x,\dot{x},z) \\ &\quad -F_{zm}(x,\dot{x})\text{sgn}(r) - k\text{sgn}(r) \\ &= -c_1 r - \tilde{\theta}\dot{x} - \tilde{m}\ddot{x}_r + \tilde{W}^T S(x,\dot{x})\text{sgn}(r) - F_z(x,\dot{x},z) \\ &\quad -F_{zm}(x,\dot{x})\text{sgn}(r) - (k - \epsilon)\text{sgn}(r) \end{aligned} \quad (3.60)$$

where $\tilde{W} = W^* - W$.

Theorem 3.4 *Consider the closed-loop system consisting of system (3.1) with dynamic friction given by (2.29) and (2.30), and adaptive controller (3.58). If the parameters $\hat{\theta}, \hat{m}$ and NN weight W are updated by*

$$\dot{\hat{\theta}} = -\eta_\theta \dot{x} r \quad (3.61)$$

$$\dot{\hat{m}} = -\eta_m \ddot{x}_r r \quad (3.62)$$

$$\dot{W} = \Gamma S(x,\dot{x})|r| \quad (3.63)$$

where η_θ and η_m are positive constants, $\Gamma = \Gamma^T > 0$ is a dimensionally compatible constant matrix, then the tracking error converges to zero and all the signals in the closed loop are bounded.

Proof Consider the candidate Lyapunov function candidate

$$V = \frac{1}{2}mr^2 + \frac{1}{2\eta_\theta}\tilde{\theta}^2 + \frac{1}{2\eta_m}\tilde{m}^2 + \frac{1}{2}\tilde{W}^T\Gamma^{-1}\tilde{W} \tag{3.64}$$

The time derivative of V along (3.60) is

$$\begin{aligned}\dot{V} &= m\dot{r}r + \frac{1}{\eta_\theta}\tilde{\theta}\dot{\tilde{\theta}} + \frac{1}{\eta_m}\tilde{m}\dot{\tilde{m}} + \tilde{W}^T\Gamma^{-1}\dot{\tilde{W}} \\ &= -c_1r^2 - \tilde{\theta}\dot{x}r - \tilde{m}\ddot{x}_r r + \tilde{W}^T S(x,\dot{x})r\mathrm{sgn}(r) + \epsilon r\mathrm{sgn}(r) \\ &\quad -F_z(x,\dot{x},z)r - F_{zm}(x,\dot{x})r\mathrm{sgn}(r) - kr\mathrm{sgn}(r) \\ &\quad +\frac{1}{\eta_\theta}\tilde{\theta}\dot{\tilde{\theta}} + \frac{1}{\eta_m}\tilde{m}\dot{\tilde{m}} + \tilde{W}^T\Gamma^{-1}\dot{\tilde{W}}\end{aligned} \tag{3.65}$$

Re-arranging the related items in (3.65) yields

$$\begin{aligned}\dot{V} &= -c_1r^2 - \tilde{\theta}(\dot{x}r - \frac{1}{\eta_\theta}\dot{\tilde{\theta}}) - \tilde{m}(\ddot{x}_r r - \frac{1}{\eta_m}\dot{\tilde{m}}) + \tilde{W}^T(S(x,\dot{x})r\mathrm{sgn}(r) \\ &\quad +\Gamma^{-1}\dot{\tilde{W}}) + \epsilon|r| - k|r| - F_z(x,\dot{x},z)r - F_{zm}(x,\dot{x})|r|\end{aligned} \tag{3.66}$$

Noting that $(\dot{\tilde{*}}) = -(\dot{\hat{*}})$ and substituting adaptation laws (3.61-3.63) into (3.66), we have

$$\dot{V} = -c_1r^2 + \epsilon|r| - k|r| - F_z(x,\dot{x},z)r - F_{zm}(x,\dot{x})|r| \tag{3.67}$$

Because $|\epsilon| \le k$ and $|F_z(x,\dot{x},z)| \le F_{zm}(x,\dot{x})$, (3.67) can be further simplified to

$$\dot{V} \le -c_1r^2 \le 0 \tag{3.68}$$

From the definition of Lyapunov function V in (3.64) and $\dot{V} \le 0$, the global uniform boundedness of the tracking error r, the parameter estimation errors $\tilde{\theta}, \tilde{m}$, and the NN weight estimation error $\tilde{W}$ are guaranteed. Obviously, the estimates $\hat{\theta}, \hat{m}$ and weight W are bounded. From the definition of r and Assumption 3.2, it can also be concluded that the tracking error e is bounded. The boundedness of the control u is apparent from (3.58).

Since $r \in L_2, e \in L_2 \cap L_\infty$, e is continuous and $e \to 0$ as $t \to \infty$, and $\dot{e} \in L_2$. By noting that $r \in L_2$ and $x_d, \dot{x}_d, \ddot{x}_d \in L_\infty$, it is concluded that $\dot{r} \in L_\infty$ from equation (3.60). Using the fact that $r \in L_2$ and $\dot{r} \in L_\infty$, thus $r \to 0$ as $t \to 0$. Hence $\dot{e} \to 0$ as $t \to 0$. $\diamondsuit$

4 Simulation Studies

In this section, simulation studies are presented to illustrate the tracking performance of the proposed adaptive friction compensators under different cases respectively. For simplicity, the system parameter is chosen as $m = 1$. The dynamic friction model given by (2.27-2.28) is used in the simulation, and the parameters are chosen as [21, 27]

$$\sigma_0 = 10^5, \sigma_1 = \sqrt{10^5}, \sigma_2 = 0.4, \dot{x}_s = 0.001, f_c = 1 \text{ and } f_s = 1.5 \tag{4.1}$$

The control objective is to make the output $x(t)$ track a desired trajectory $x_d(t) = 0.5\sin(2\pi t)$. The initial states are $[x(0), \dot{x}(0)]^T = [0.1, 0]^T$. The filtered tracking error $r = \dot{e} + \lambda e, \lambda = 5, e = x - x_d$, and $\ddot{x}_r = \ddot{x}_d - \lambda\dot{e}$.

In the following, we shall show the tracking results for the case of LIP friction model based design and the case of dynamic LuGre friction model based design. First, we consider the case where the complex friction behavior is approximated by the LIP static friction model presented in Section 2.1, and present the performance of the corresponding model based adaptive control algorithms proposed in Section 3.2. Both model based and neural network based adaptive friction compensation results are comparatively illustrated. Secondly, based on the uncertainty levels with the dynamic LuGre model (2.29-2.30), the proposed adaptive friction compensation controllers in Section 3.3 are verified by the simulation results. Finally, some concluding remarks are given on the performance of the adaptive friction compensation schemes proposed in this chapter.

4.1 Static Model Based Adaptive Control

In this subsection, we shall study the performance of the static model based adaptive control. As shown in Section 2.1, basic friction behavior can be captured by conventional LIP static friction model (2.15) or NN based LIP static friction model (2.20).

4.1.1 Conventional LIP model based adaptive control

For analysis, the conventional LIP friction models used in the simulation are in the form $F(x, \dot{x}) = S^T(\dot{x})P$ with the following different choice of $S(\dot{x})$ and P:

(1) $S(\dot{x}) = \text{sgn}(\dot{x})$, $P = f_c$;
(2) $S(\dot{x}) = [\text{sgn}(\dot{x}), \dot{x}]^T$, $P = [f_c, f_v]^T$;
(3) $S(\dot{x}) = [\text{sgn}(\dot{x}), \dot{x}, |\dot{x}|\dot{x}]^T, P = [f_c, f_v, f_d]^T$;
(4) $S(\dot{x}) = [\text{sgn}(\dot{x}), \dot{x}, |\dot{x}|\dot{x}, |\dot{x}|^{1/2}\text{sgn}(\dot{x})]^T$, $P = [f_c, f_v, f_d, f_r]^T$.

The corresponding adaptive controller is given by (3.8), i.e.,

$$u = -k_1 r + \hat{m}\ddot{x}_r + S^T(\dot{x})P - k_i \int_0^t r d\tau - u_r \tag{4.2}$$

where $k_i = 0$, $u_r = k_2 \text{sgn}(r)$ with $k_2 = 2$, and $k_1 = 10$ for cases 1 and 2 while $k_1 = 80$ for cases 3 and 4. The adaptation gain is chosen as $\Gamma = \text{diag}[0.1]$ for cases 1 and 2, and $\Gamma = \text{diag}[10]$ for cases 3 and 4. The tracking performance is shown in Figure 4.1, while the control signals are shown in Figure 4.2.

It was found that the system becomes unstable for high-gain feedback because the friction models are too simple to sufficiently approximate the LuGre model in the plant. The allowable feedback gain is $k_1 = 10$ for cases 1 and 2, and large tracking errors exist. Because of the existence of large tracking errors, the gain of adaptation cannot be chosen too large either. If a high adaptive gain is chosen, the system may become unstable.

For cases 3 and 4, as the friction models become complex and capture the dominate dynamics behaviors, it was found the high feedback gains can be used and the speed of adaptation can also be increased. For comparison studies, the tracking performance is also shown in Figure 4.1, while the control signals are shown in Figure 4.2 when $k_1 = 80$ and $\Gamma = \text{diag}[10]$. It can be seen that tracking performance become much better. The boundedness of the adaptive parameters are shown in Figure 4.3.

4.1.2 NN LIP model based adaptive control

RBF NN $F(x, \dot{x}) = S^T(x, \dot{x})W$ is used as the friction model, and the corresponding adaptive controller is also given by (3.8), i.e.,

$$u = -k_1 r + \hat{m}\ddot{x}_r + S^T(\dot{x})W - u_r - k_i \int_0^t r d\tau \tag{4.3}$$

where $k_1 = 10$, $k_i = 0$, $u_r = k_2 \text{sgn}(r)$ with $k_2 = 2$. The adaptation gain is chosen as $\Gamma = \text{diag}[100]$.

To show the effectiveness of NN-based adaptive control, a Gaussian RBF neural network of 100 nodes is chosen to approximate friction with $\sigma^2 = 10.0$.

The tracking performance is shown in Figure 4.4, while the control signals and neural network weights are shown in Figure 4.5 and Figure 4.6, respectively.

It can be seen that a NN LIP model based adaptive controller can produce good tracking performance and guarantees the boundedness of all the closed-loop signals because the neural network friction model can capture the dynamic behavior of the LuGre model in the plant.

4.2 Dynamic LuGre Friction Model Based Adaptive Control

In this subsection, we study the performance of the adaptive friction compensation schemes proposed in Section 3.2 based on different uncertainty levels of dynamic LuGre friction.

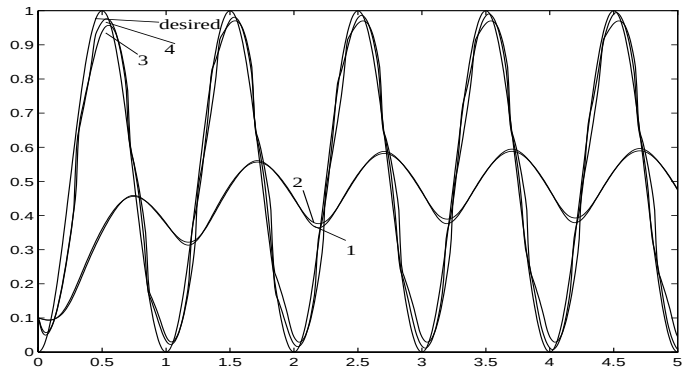

Fig. 4.1. Tracking performance of conventional LIP model based adaptive control.

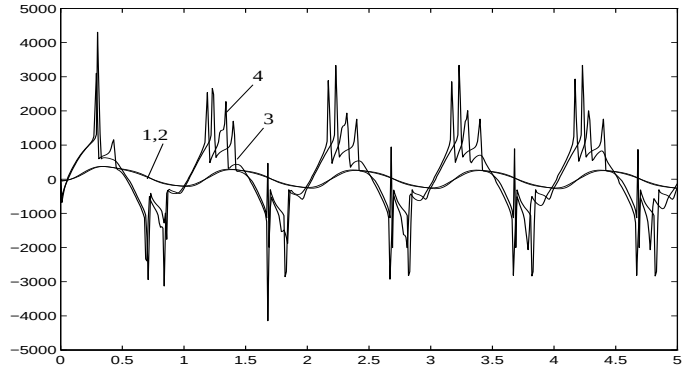

Fig. 4.2. Control signals of conventional LIP model based adaptive control.

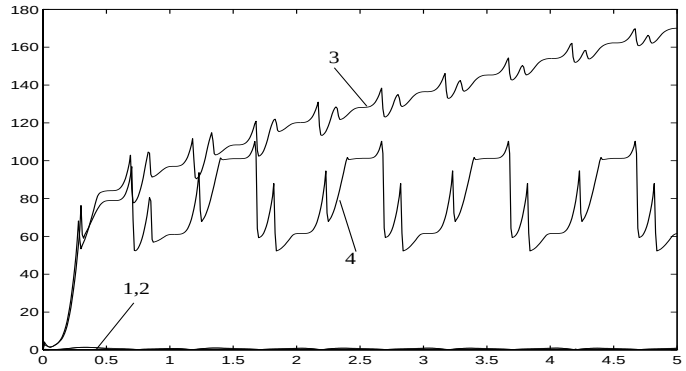

Fig. 4.3. Variations in parameters.

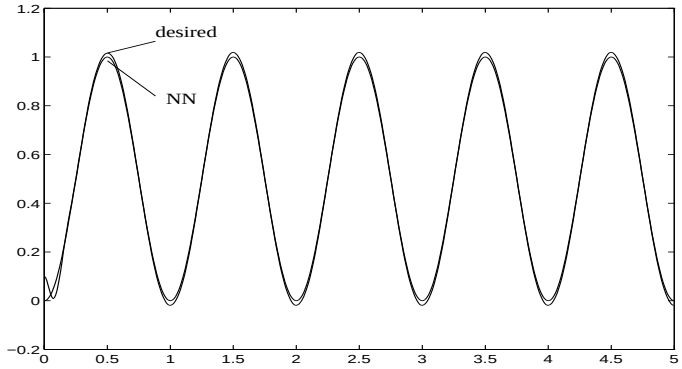

Fig. 4.4. Tracking performance of NN LIP model based adaptive control.

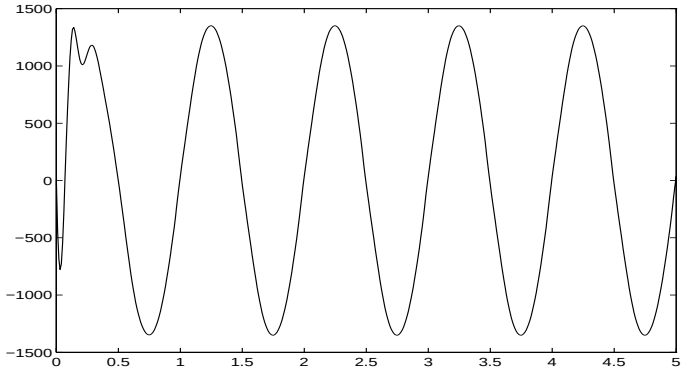

Fig. 4.5. Control signals of NN LIP model based adaptive control.

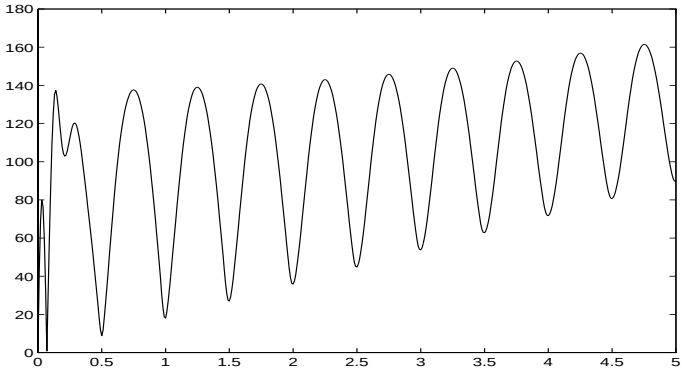

Fig. 4.6. Variations in NN weights.

4.2.1 Adaptive control for unknown system parameters

The system parameter m and dynamic friction parameters $\sigma_0, \sigma_1, \sigma_2$ are assumed unknown while nonlinear function $\alpha(x, \dot{x})$ is given by (2.28). The corresponding adaptive controller is given by (3.25), i.e.,

$$u = -c_1 r + \hat{\sigma}_1 \dot{x} + \hat{\sigma}_2 \dot{x} + \hat{\sigma}_0 \hat{z}_0 - \alpha(x, \dot{x}) \hat{\sigma}_1 |\dot{x}| \hat{z}_1 + \hat{m} \ddot{x}_r \tag{4.4}$$

where $c_1 = 50$, $\hat{z}_0$ and $\hat{z}_1$ are the outputs of the observers (3.23) and (3.24) respectively. The adaptation gains are chosen as $\eta_0 = 10, \eta_1 = 10, \eta_2 = 10$ and $\eta_m = 10$. Figure 4.7 and Figure 4.8 show that both the actual position and velocity outputs asymptotically track the desired system trajectory and velocity outputs. The bounded dual-observer outputs and the actual internal dynamic friction state z are shown in Figure 4.10. It can be seen from Figure 4.10 that (i) the output $\hat{z}_0$ of the first observer is roughly the same as the actual internal friction state z, and (ii) the output $\hat{z}_1$ of the second observer is not at the same scale with z though bounded. This is due to the different purposes of the two observers. The first one is mainly for friction state estimation and the second one can be regarded as an auxiliary signal used to cancel the cross-coupling terms in the derivative of the Lyapunov function for closed-loop stability. Figure 4.9 indicates the bounded control signal u. The boundedness of the estimated parameters is illustrated in Figure 4.11.

4.2.2 Adaptive control for unknown $\alpha(x, \dot{x})$

The parameters m, σ_0, σ_1 and σ_2 are known while the nonlinear function $\alpha(x, \dot{x})$ is unknown. The RBF NN $\hat{\alpha}(x, \dot{x}) = W^T S(x, \dot{x})$ is used to approximate the unknown $\alpha(x, \dot{x})$. The NN is chosen of size $l = 49$, variance $\sigma = 1$, centers $\mu_i = [\mu_{i1}, \mu_{i2}]^T, i = 1, 2, \cdots, l$ covering all the 49 combinations of $\mu_{i1} = \{-1.5, -1, -0.5, 0, 0.5, 1, 1.5\}$ and $\mu_{i2} = \{-10, -5, -2.5, 0, 2.5, 5, 10\}$. The initial conditions for NN are $W(0) = 0$. The corresponding adaptive controller is given by (3.45-3.46), i.e.,

$$u = (\sigma_1 + \sigma_2)\dot{x} + m\ddot{x}_r + u_{ar} \tag{4.5}$$

with

$$\begin{aligned} u_{ar} \quad = \quad & -c_1 r + \sigma_0 \hat{\delta}_1 - \sigma_1 \hat{\alpha}(x, \dot{x}) |\dot{x}| \hat{\delta}_2 - \frac{m\sigma_0}{\sigma_1} r - \frac{\sigma_1^2 \sigma_2 \alpha_m r \dot{x}^2}{\sigma_0} \\ & -k\sigma_1 |\dot{x}| |\hat{\delta}_2| \mathrm{sgn}(r) \end{aligned} \tag{4.6}$$

where the control parameters are chosen as $c_1 = 30, k = 10$. From the parameterization of $\alpha(x, \dot{x})$ in equation (2.28), we have $0 < \alpha(\dot{x}) \leq \frac{\sigma_0}{f_c} = 10^5$. Accordingly, we choose $\alpha_m = \frac{\sigma_0}{f_c} = 10^5$ in the simulation. The adaptation gain for NN weights is chosen as $\Gamma = 10$. Figure 4.12 and Figure 4.13 show that good position and velocity tracking performances are achieved. Figure 4.14 indicates the bounded control signal u. The bounded dual-observer outputs and the actual value of the auxiliary variable $\delta = z + \frac{m}{\sigma_1} r$ are illustrated in

Figure 4.15. It can be seen from Figure 4.15 that (i) the output $\hat{\delta}_1$ of the first observer is roughly the same as the actual friction state δ, and (ii) the output $\hat{\delta}_2$ of the second observer is not at the same scale as δ though bounded. This is due to the fact that the first observer is for friction state estimation and the second one is an auxiliary signal for the cancelation of the cross-coupling term in the derivative of the Lyapunov function. Figure 4.16 presents the boundedness of NN weights.

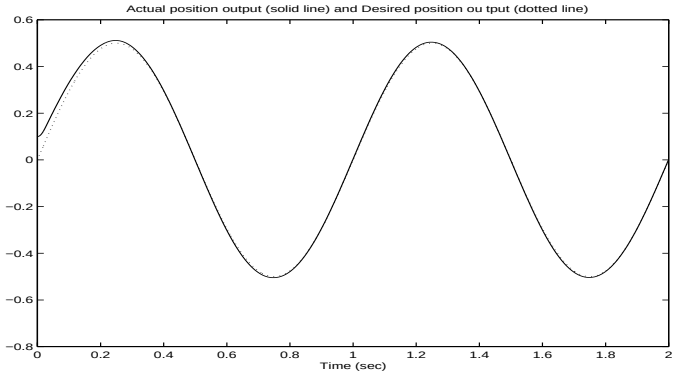

Fig. 4.7. Position tracking performance of Case 1.

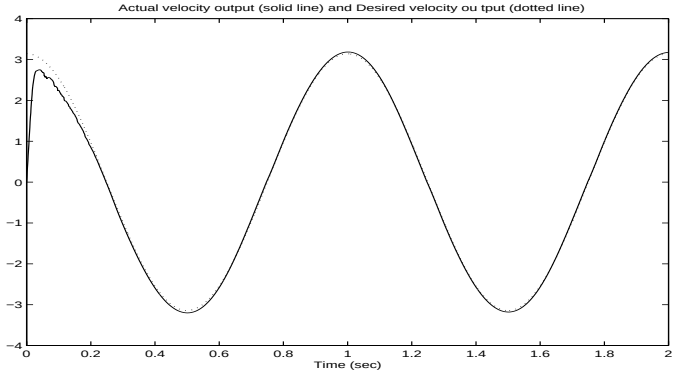

Fig. 4.8. Velocity tracking performance of Case 1.

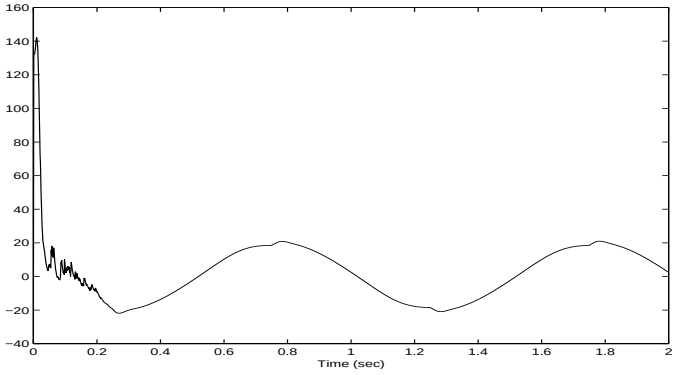

Fig. 4.9. Control input of Case 1.

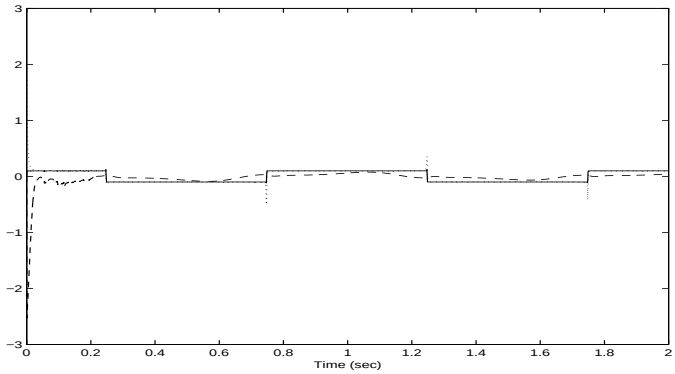

Fig. 4.10. Dual-observer outputs of Case 1 ($z * 10^4$: solid line; $\hat{z}_0 * 10^4$: dotted line; $\hat{z}_1$: dashed line).

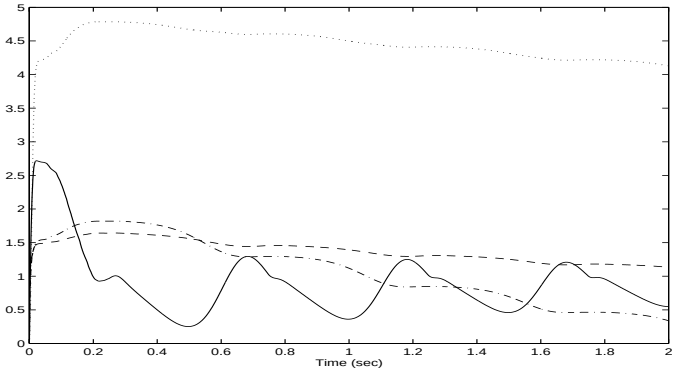

Fig. 4.11. Parameter estimates of Case 1 ($\hat{m}$: solid line; $\hat{\sigma}_0$: dashed line; $\hat{\sigma}_1$: dotted line; $\hat{\sigma}_2$: dashdot line).

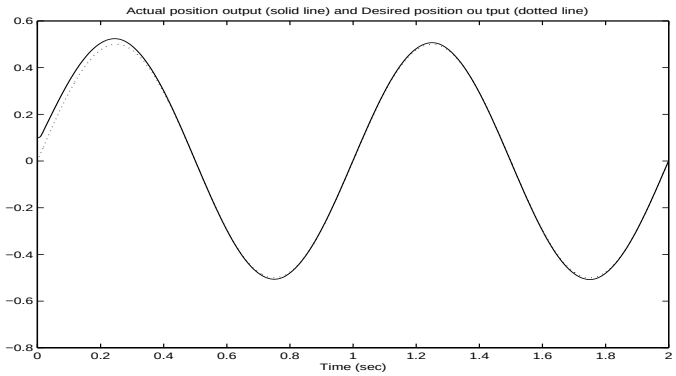

Fig. 4.12. Position tracking performance of Case 2.

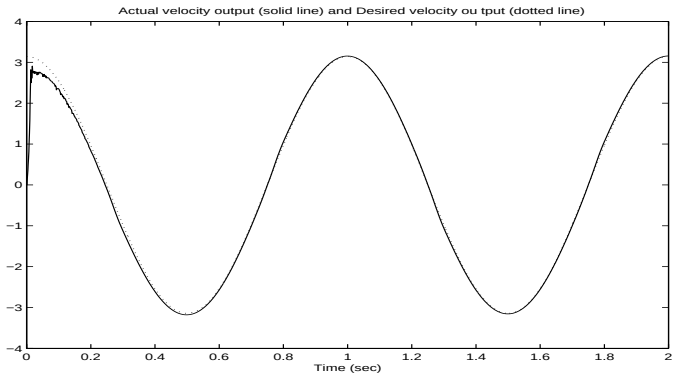

Fig. 4.13. Velocity tracking performance of Case 2.

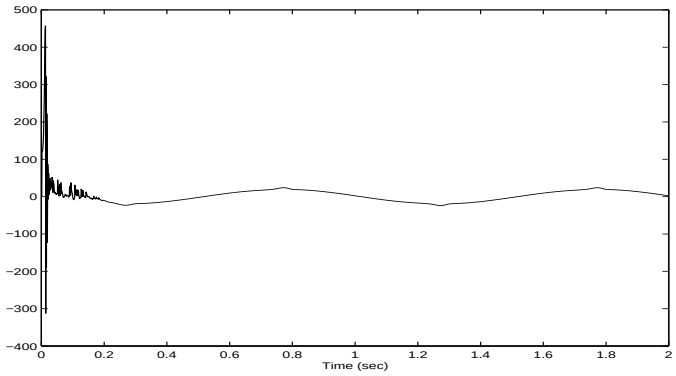

Fig. 4.14. Control input of Case 2.

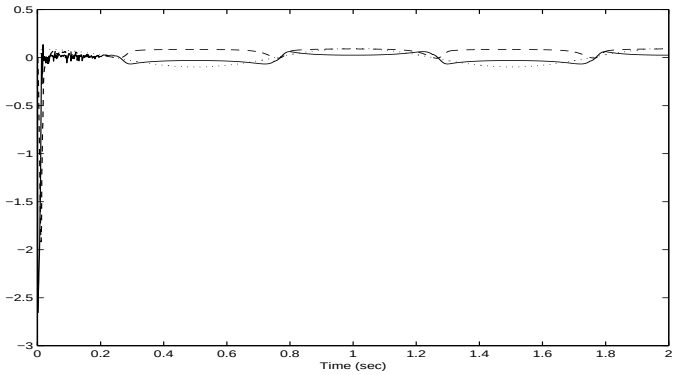

Fig. 4.15. Dual-observer outputs of Case 2 (δ*10: solid line; $\hat{\delta}_1$*10: dotted line; $\hat{\delta}_2$: dashed line).

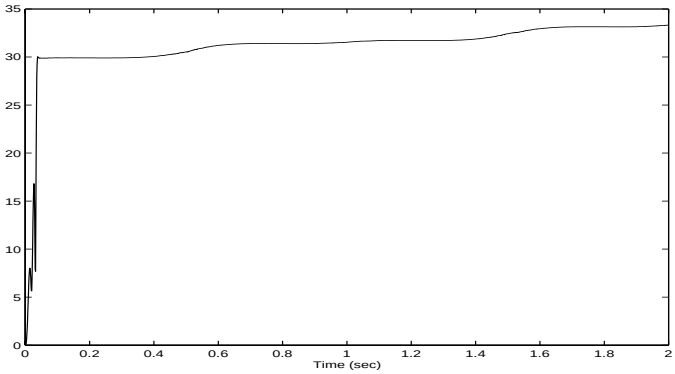

Fig. 4.16. Norm of estimated weights $\|W\|$ of Case 2.

4.2.3 Adaptive control for full set of unknown parameters

In this case, the full set of system and friction model parameters are assumed unknown. The RBF NN $\hat{F}_{zm}(x,\dot{x}) = W^T S(x,\dot{x})$ is used to approximate the function bound $F_{zm}(x,\dot{x})$. The NN is chosen of size $l = 25$, variance $\sigma = 1$, centers $\mu_i = [\mu_{i1}, \mu_{i2}]^T, i = 1, 2, \cdots, l$ covering all the 25 combinations of $\mu_{ij} = \{-1, -0.5, 0, 0.5, 1\}, j = 1, 2$. The initial conditions for NN are $W(0) = 0$. The corresponding adaptive controller is given by (3.58), i.e.,

$$u = -c_1 r + \hat{\theta}\dot{x} + \hat{m}\ddot{x}_r - \hat{F}_{zm}(x,\dot{x})\text{sgn}(r) - k\text{sgn}(r) \tag{4.7}$$

where the control parameters are chosen as $c_1 = 50, k = 10$. The adaptation gains are chosen as $\Gamma = 10, \eta_\theta = 10$ and $\eta_m = 10$. Figure 4.17 and Figure 4.18 respectively show the ideal position and velocity tracking performance. Figure 4.19 indicates the bounded control signal u. Figure 4.20 presents the boundedness of NN weights, and the bounded parameter estimation results are illustrated in Figure 4.21.

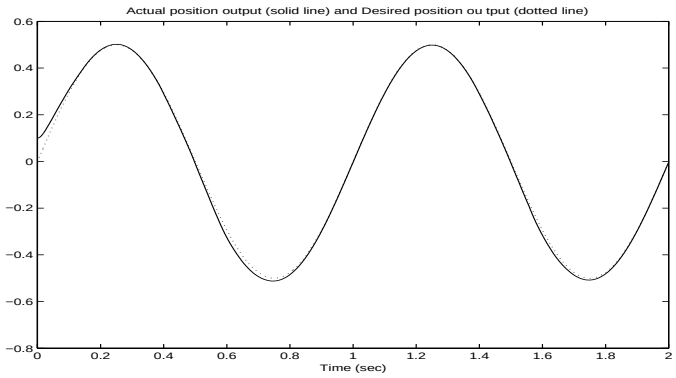

Fig. 4.17. Position tracking performance of Case 3.

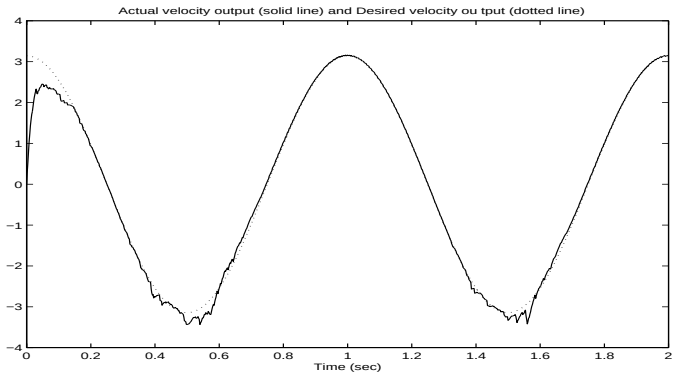

Fig. 4.18. Velocity tracking performance of Case 3.

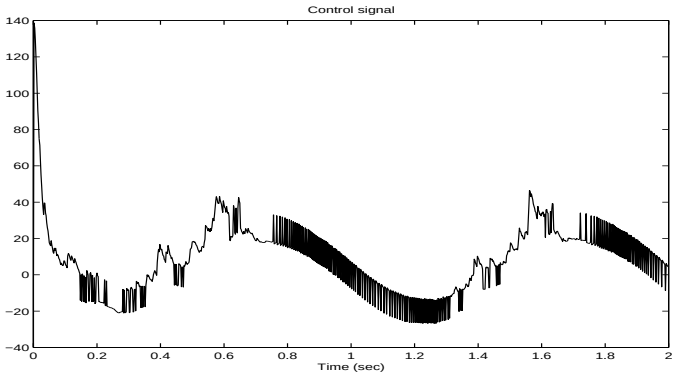

Fig. 4.19. Control input of Case 3.

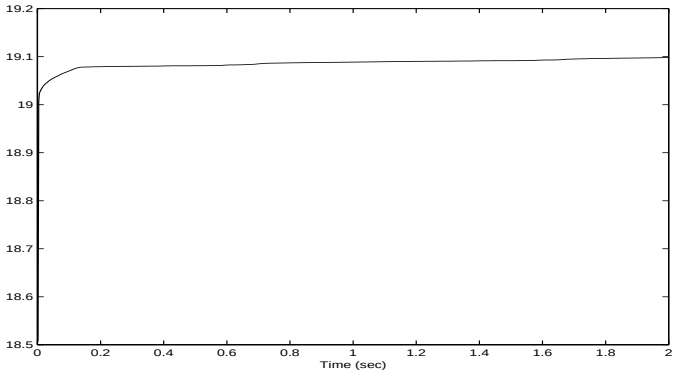

Fig. 4.20. Norm of estimated weights $\|W\|$ of Case 3.

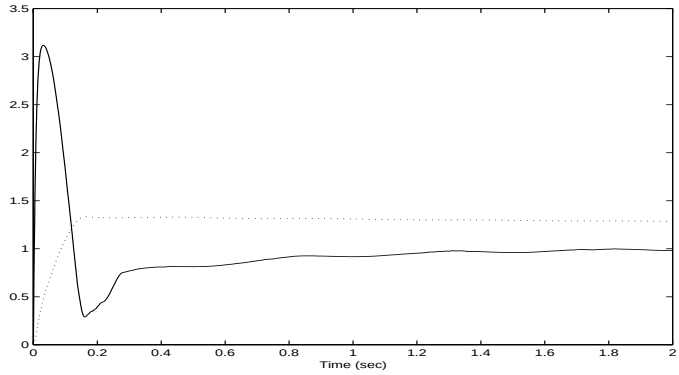

Fig. 4.21. Parameter estimates of Case 3 ($\hat{m}$: solid line; $\hat{\theta}$: dotted line).

Remark 4.1. From the simulation results in Section 4.1 and Section 4.2, it can easily be found that the performance of dynamic LuGre model based adaptive control is better than the results of LIP model based adaptive control. This is because the dynamic LuGre friction model more accurately captures the complex static and dynamic characteristics of friction. High precision motion control can be achieved by using the dynamic LuGre model based adaptive control schemes proposed in Section 3.2.

Remark 4.2. For conventional LIP model based adaptive control, we found from Figure 4.1 that by augmenting the basis function space to capture the dynamics of friction more accurately, better performance can be obtained. In fact, systems with simpler friction models may become unstable for high-gain feedback, and the gain of adaptation cannot be chosen too large either, whereas for systems with complex friction models it was found that high feedback gains can be used and the speed of adaptation can also be increased.

Remark 4.3. For NN LIP model based adaptive control, though better performance is obtained compared with conventional LIP model base adaptive control results, its performances is worse than that of the dynamic LuGre model based adaptive control. The reason is that the complex friction structure uncertainty is not revealed by direct NN approximation.

Remark 4.4. All of the results for dynamic LuGre model based adaptive control are ideal as shown in Section 4.2. However, the first two methods need the assumption of partially known friction model parameters, which may be hard to meet in practice. These assumptions are relaxed in the third approach without any sacrifice in performance.

5 Conclusion

In this chapter, a systematic treatment of adaptive friction compensation techniques has been presented. First, the commonly used static friction models and dynamic friction models were detailed using the corresponding model features analysis. Then, by considering the position and velocity tracking control of a servo mechanism with friction, adaptive friction compensation schemes are given based on the proposed LIP static friction model and dynamic LuGre friction model respectively. Using Lyapunov synthesis, adaptation algorithms were designed to achieve asymptotic tracking of the desired trajectory and guarantee the boundedness of all signals in the closed loop. Both position tracking and velocity tracking were realized at the same time by utilization of a filtered error signal. Extensive numerical simulation results have shown that the proposed approaches are effective for friction compensation in servo mechanisms.

References

1. A. M. Annaswamy, F. P. Skantze and A. P. Loh, Adaptive control of continuous time systems with convex/concave parameterization, *Automatica*, 34, no. 1, 33-49, 1998.
2. B. Armstrong, Friction experimental determination, modeling and compensation, *IEEE Int. Conf. Robotics and Automation*, pp. 1422-1427, 1988.
3. B. Armstrong, Stick-slip arising from stribeck friction, *IEEE Int. Conf. Robotics and Automation*, Cincinnati, pp. 1377-1382, 1990.
4. B. Armstrong-Helouvry, P. Dupont and C. Canudas de Wit, A survey of analysis tools and compensation methods for the control of machines with friction, *Automatica*, 30, no. 7, 1083-1138, 1994.
5. B. Armstrong and B. Amin, PID control in the presence of static friction: a comparison of algebraic and describing function analysis, *Automatica*, 32, no. 5, 679-692, 1996.
6. N. Barabanov and R. Ortega, Necessary and sufficient conditions for passivity of the LuGre friction model, *Proc. of IFAC 14 World Congress*, Beijing, pp. 399-402, 1999.
7. L. C. Bo and D. Pavelescu, The friction-speed relation and its influence on the critical velocity of the stick-slip motion, *Wear*, 3, 277-289, 1982.
8. L. Cai and G. Song, A smooth robust nonlinear controller for robot manipulators with joint job stick-slip friction, *Proc. IEEE Int. Conf. Robotics Automation*, Atlanta, GA, pp. 449-454, 1993.
9. L. Cai and G. Song, Joint stick-slip friction compensation of robot manipulators by using smooth robust controller, *J. of Robotic Systems*, 11, no. 6, 451-470, 1994.
10. C. Canudas de Wit, K. J. Åström and K. Brawn, Adaptive friction compensation in DC motor drives, *IEEE J. of Robotics and Automation*, 3, no. 6, 681-685, 1987.

11. C. Canudas De Wit and J. Carillo, A modified EW-RLS algorithm for system with bounded disturbance, *Automatica*, 26, no. 4, 599-606, 1990.
12. C. Canudas de Wit, C. P. Noel, A. Auban and B. Brogliato, Adaptive friction compensation in robot manipulators: low velocities, *Int. J. of Robotics Research*, 10, no. 3, 189-199, 1991.
13. C. Canudas de Wit, H. Olsson, K. J. Åström and P. Lischinsky, A new model for control of systems with friction, *IEEE Trans. on Automatic control*, 40, no. 3, 419-425, 1995.
14. C. Canudas de Wit and S. S. Ge, Adaptive friction compensation for systems with generalized velocity/position friction dependency, *Proceedings of the 36th IEEE Conf. on Decision and Control*, San Diego, CA, pp. 2465-2470, 1997.
15. C. Canudas de Wit and P. Lischinsky, Adaptive friction compensation with partially known dynamic friction model, *Int. J. of Adaptive Control & Signal Processing*, 11, 65-80, 1997.
16. T. P. Chen and H. Chen, Approximation capability to functions of several variables, nonlinear functionals, and operators by radial basis function neural networks, *IEEE Trans. Neural Networks*, 6, no. 4, 904-910, 1995.
17. P. R. Dahl, A solid friction model, *Report AFO 4695-67-C-0158*, Aerospace Corporation, EI Segundo, California, 1968.
18. P. E. Dupont, Avoiding stick-slip through PD control, *IEEE Trans. on Automatic Control*, 39, no. 5, 1094-1097, 1994.
19. B. Friedland and Y. J. Park, On adaptive friction compensation, *IEEE Trans. on Automatic Control*, 37, no. 10, 1609-1612, 1992.
20. S. S. Ge, T. H. Lee and C. J. Harris, Adaptive Neural Network Control of Robot Manipulators, World Scientific, River Edge, NJ, 1998.
21. S. S. Ge, T. H. Lee and S. X. Ren, Adaptive friction compensation of servo mechanisms, *Int. J. of Systems Sciences*, to appear, 2001.
22. S. S. Ge, T. H. Lee and J. Wang, Adaptive NN Control of Dynamic Systems with Unknown Dynamic Friction, *Proceedings of the 39th IEEE Conf. on Decision and Control*, Sydney, Dec. 12-15, 2000.
23. D. P. Hess and A. Soom, Friction at a lubricatal line contact operating at oscillating sliding velocity, *J. Tribology*, 112, no. 1, 147-152, 1990.
24. P. A. Ioannou and J. Sun, *Robust Adaptive Control*, Prentice-Hall, Upper Saddle River, NJ, 1996.
25. Y. H. Kim and F. L. Lewis, Reinforcement adaptive learning neural-net-based friction compensation control for high speed and precision, *IEEE Trans. on Control Systems Technology*, 8, no. 1, 118-126, 2000.
26. F. L. Lewis and K. Liu, Multilayer neural-net robot controller with guaranteed tracking performance, *IEEE Trans. on Neural Network*, 7, 188-198, 1996.
27. K. M. Misovec and A. M. Annaswamy, Friction compensation using adaptive nonlinear control with persistent excitation, *Int. J. Control*, 72, no. 5, 457-479, 1999.
28. H. Olsson, K. J. Åström, C. Canudas de wit, M. Gafvert and P. Lischinsky, Friction models and friction compensation, *European Journal of Control*, 4, 176-195, 1998.
29. R. Ortega, A. Loria, P. J. Nicklasson and H. Sira-Ramirez, Passivity-based Control of Euler-Lagrange Systems, Springer-Verlag, London, 1998

30. T. Poggio and F. Girosi, Networks for approximation and learning. *Proc. of IEEE*, 78, 1481-1497, 1990.

31. M. M. Polycarpou and P. A. Ioannou, A robust adaptive nonlinear control design, *Proceedings of ACC*, San Francisco, CA, pp. 1365-1369, 1993.

32. Y. Tan and I. Kanellakopoulos, Adaptive nonlinear friction compensation with parametric uncertainties, *Proceedings of ACC*, San Diego, CA, pp. 2511-2515, 1999.

33. A. Tustin, The effects of backlash and of speed-dependent friction on the stability of closed-cycle control system, *J. Institution of Electrical Engineers*, 94, no. 2, 143-151, 1947.

34. S. Ward, S. C. Radcliff and C. J. MacCluer, Robust nonlinear stick-slip friction compensation, *ASME Journal of Dynamic Systems, Measurement, and Control*, 113, 639-645, 1991.

35. A. Tustin, The effects of backlash and of speed-dependent friction on the stability of closed-cycle control system, *J. Institution of Electrical Engineers*, 94, no. 2, 143-151, 1947.

36. T. Zhang, S. S. Ge and C. C. Hang, "Design and performance analysis of a direct adaptive controller for nonlinear systems", *Automatica*, 35, no. 11, 1809-1817, 1999.